AFRL-RV-PS-
TR-2016-0123

AFRL-RV-PS-
TR-2016-0123

WIDEBAND FM DEMODULATION AND MULTIRATE FREQUENCY TRANSFORMATIONS

Balu Santhanam and Wenjing Liu

University of New Mexico
1700 Lomas Blvd NE
Albuquerque, NM 87106-3807

15 Dec 2016

Final Report

APPROVED FOR PUBLIC RELEASE; DISTRIBUTION IS UNLIMITED.

AIR FORCE RESEARCH LABORATORY
Space Vehicles Directorate
3550 Aberdeen Ave SE
AIR FORCE MATERIEL COMMAND
KIRTLAND AIR FORCE BASE, NM 87117-5776

DTIC COPY
NOTICE AND SIGNATURE PAGE

AFRL-RV-PS-TR-2016-0123 HAS BEEN REVIEWED AND IS APPROVED FOR PUBLICATION IN ACCORDANCE WITH ASSIGNED DISTRIBUTION STATEMENT.

//SIGNED//
DAVID MURRELL
Program Manager

//SIGNED//
DAVID CARDIMONA
Technical Advisor, Space Based Advanced Sensing and Protection

//SIGNED//
JOHN BEAUCHEMIN
Chief Engineer, Spacecraft Technology Division
Space Vehicles Directorate

REPORT DOCUMENTATION PAGE

Form Approved OMB No. 0704-0188

1. REPORT DATE *(DD-MM-YY)* 15-12-2016	**2. REPORT TYPE** Final Report	**3. DATES COVERED** *(From - To)* 1 May 2014 – 30 Oct 2016

4. TITLE AND SUBTITLE Wideband FM Demodulation and Multirate Frequency Transformations	**5a. CONTRACT NUMBER** FA9453-14-1-0234
	5b. GRANT NUMBER
	5c. PROGRAM ELEMENT NUMBER 62601F
6. AUTHOR(S) Balu Santhanam and Wenjing Liu	**5d. PROJECT NUMBER** 8809
	5e. TASK NUMBER PPM00019616
	5f. WORK UNIT NUMBER EF122380
7. PERFORMING ORGANIZATION NAME(S) AND ADDRESS(ES) University of New Mexico 1700 Lomas Blvd NE Albuquerque, NM 87106-3807	**8. PERFORMING ORGANIZATION REPORT NUMBER**
9. SPONSORING / MONITORING AGENCY NAME(S) AND ADDRESS(ES) Air Force Research Laboratory Space Vehicles Directorate 3550 Aberdeen Ave., SE Kirtland AFB, NM 87117-5776	**10. SPONSOR/MONITOR'S ACRONYM(S)** AFRL/RVSW
	11. SPONSOR/MONITOR'S REPORT NUMBER(S) AFRL-RV-PS-TR-2016-0123

12. DISTRIBUTION / AVAILABILITY STATEMENT
Approved for public release; distribution is unlimited.

13. SUPPLEMENTARY NOTES

14. ABSTRACT
Conventional narrowband demodulation approaches assume that the signal of interest is narrowband, i.e., with bandpass spectral content confined to a bandwidth that is much smaller in comparison to the carrier frequency. However if the signal of interest is a wideband signal, the underlying assumptions are violated and these approaches incur significant demodulation error. In this report, we summarize the proposed wideband demodulation approach that employs multirate frequency transformations to convert the wideband signal to a narrowband signal so that conventional demodulation algorithms can be applied. The information signals associated with the wideband input are obtained via the inverse multirate frequency transformation. We then outline an approach that employs multirate Noble identities to extend the proposed approach to larger wideband to narrowband conversion factors and more practical implementations. We further detail its application to the associated problems of wideband image demodulation, wideband speech formant demodulation, and wideband demodulation. These applications demonstrate the efficacy of the wideband demodulation approach.

15. SUBJECT TERMS
RF; Processing; Communications; Demodulation Algorithms

16. SECURITY CLASSIFICATION OF:			**17. LIMITATION OF ABSTRACT**	**18. NUMBER OF PAGES**	**19a. NAME OF RESPONSIBLE PERSON** David Murrell
a. REPORT Unclassified	**b. ABSTRACT** Unclassified	**c. THIS PAGE** Unclassified	Unlimited	52	**19b. TELEPHONE NUMBER** *(include area code)*

Standard Form 298 (Rev. 8-98)
Prescribed by ANSI Std. 239.18

(This page intentionally left blank)

Table of Contents

List of Figures

List of Tables

1 Summary

Conventional narrowband FM demodulation approaches assume that the signal of interest is narrowband, i.e., with bandpass spectral content confined to a bandwidth that is much smaller in comparison to the carrier frequency. However if the signal of interest is a wideband FM signal, the underlying assumptions are violated and these approaches incur significant demodulation error.

In this report, we summarize the proposed wideband AM–FM demodulation approach that employs multirate frequency transformations to convert the wideband FM signal to a narrowband signal so that conventional demodulation algorithms can be applied. The information signals associated with the wideband input are obtained via the inverse multirate frequency transformation.

We then outline an approach that employs multirate Noble identities to extend the proposed approach to larger wideband to narrowband conversion factors and more practical implementations. We further detail its application to the associated problems of wideband FM image demodulation, wideband speech formant demodulation, and wideband CPM demodulation. These applications demonstrate the efficacy of the MFT based wideband demodulation approach.

2 Introduction

Existing conventional narrowband FM demodulation approaches such as the Hilbert transform approach [1] or the Teager-Kaiser operator based energy separation algorithm [2] assume that the information bandwidth of the communications is much smaller in comparison to the carrier frequency of the signal. When this condition is not met, specifically when the signal of interest is wideband, they incur significant demodulation error. Such wideband FM signals are encountered in satellite communications [3] or in the form of hypernasal signals encountered in people with cleft lip or palate situations.

In recent work [4], multirate frequency transformations (MFT), were proposed as a mechanism for converting wideband FM signals into narrowband signals so that conventional demodulation approached may be applied. The estimated information signals are then inverse transformed to obtain the information signals associated with the original wideband input.

In this report, we outline the extension of this approach to larger wideband to narrowband conversion factors, thereby enabling more practical implementations of the MFT approach. We further detail the application of the MFT based wideband FM demodulation approach to the associated problems of: (a) wideband image demodulation, (b) wideband nasal formant demodulation, and (c) wideband continuous phase modulation (CPM) demodulation for satellite communications.

2.1 AM-FM Signal Model

Monocomponent amplitude-modulation frequency-modulation (AM-FM) signals are time-varying sinusoids of the form:

$$s\left(t\right) = a(t)\cos\left(\int_{-\infty}^{t} \omega_i\left(\tau\right) d\tau + \theta_1\right), \tag{1}$$

where instantaneous amplitude (IA) is denoted by $a(t)$ and the instantaneous frequency (IF) is given by

$$\omega_i(t) = \omega_c + \omega_m q_i(t). \tag{2}$$

Note that w_c is the carrier (or mean) frequency and $q_i(t)$ is the normalized baseband modulated signal.

Specific for sinusoidal FM, where $a(t)$ remains a constant A, and $q_i(t)$ becomes a sinusoid, the IF can be further expressed as

$$\omega_i(t) = \omega_c + \omega_m \cos(\omega_f t + \theta_2). \tag{3}$$

Sinusoidal FM signals can be expressed via Bessel functions as:

$$s(t) = A \sum_{n=-\infty}^{+\infty} J_n(\beta) \cos(\omega_c t + n\omega_m t), \tag{4}$$

where J_n is the n^{th} order cylindrical Bessel function of the first kind. The modulation index of the sinusoidal FM is defined as the ratio $\beta = \omega_m/\omega_f$ and the associated carson's bandwidth is given by

$$B = 2(\beta + 1)\omega_f. \tag{5}$$

If $\beta \gg 1$, then it corresponds to the wideband FM according to the literature of FM communication systems. In addition, the carrier-to-information-bandwidth ratio (CR/IB) and the carrier-to-frequency deviation ratio (CR/FD) are defined respectively as:

$$\frac{CR}{IB} = \frac{\omega_c}{\omega_f}, \quad \frac{CR}{FD} = \frac{\omega_c}{\omega_m}. \tag{6}$$

2.2 Conventional Demodulation Approaches

In this section, we briefly overview three conventional demodulation approaches. Note that the adaptive linear predictive IF tracking are intended for FM signals only, whereas the analytic signal (AS) approach based on the Hilbert transform (HT) and the *energy separation algorithm* (ESA) are intended for AM-FM signals.

2.2.1 Adaptive Linear Predictive IF Tracking

For a pure FM signal, the IF demodulation approach employing adaptive filters was proposed in prior work [4]. According to the Wiener-Hopf equations [5], the optimal coefficients of a linear predictor are given by

$$\mathbf{w}^{opt} = \mathbf{R}_{xx}^{-1}\mathbf{r}_{dx}, \tag{7}$$

where $\mathbf{w}^{opt}$ denotes the optimal tap weight vector, $\mathbf{R}_{xx}$ denotes the input correlation matrix and $\mathbf{r}_{dx}$ denotes the cross-correlation between input vector and desired signal. As summarized in [5], the prediction error filter is given by:

$$E(z) = 1 - \sum_{l=1}^{L} g_l^{opt} z^{-l}, \tag{8}$$

where $\left\{g_l^{opt}\right\}_{l=1}^{L}$ are the coefficients of the corresponding optimal predictor. Conditioned on the small prediction error assumption and the further assumption that the message signal remains essentially invariant over the sampling range of the linear prediction filter, we end up with the approximation in [6] through (8) given by

$$\sum_{l=1}^{L} g_l\left(k\right) \exp\left\{-jl\left[w_c + m\left(k\right)\right]\right\} \simeq 1, \tag{9}$$

where $g_l(k)$ is the weight coefficient of tap l at time index k and $m(k)$ is the sample of the message signal at time index k. Then the IF of the signal of interest can be estimated by executing the following steps: 1) Compute the coefficients of the prediction error filter; 2) Obtain the roots of the coefficient polynomial; 3) Calculate the phase argument of the complex conjugate pole location of the corresponding roots.

In the prior work, adaptive algorithms such as AS-LMS (Analytic Signal Least Mean Square) and AF-RLS (Root Least Squares) have been incorporated into the structure of a linear predictor and compared with each other based on the demodulation error. However, for both algorithms, the step-size or the forgetting factor needs to be truncated to remain within certain range. Here we choose the generalized normalized gradient descent (GNGD) [7] for update of the linear predictor coefficients, which avoids truncation of the adaptively adjusted step-size. The algorithm for this GNGD linear predictive filter is summarized via

$$e\left(k\right) = x\left(k+1\right) - \sum_{l=1}^{L} g_l\left(k\right) x\left(k-L+1\right), \tag{10}$$

$$\beta\left(k\right) = \beta(k-1) - \rho\alpha\frac{e(k)e(k-1)\mathbf{x}^T(k)\mathbf{x}(k-1)}{(\|\mathbf{x}(k)\|_2^2 + \beta(k))^2}, \tag{11}$$

$$\eta\left(k\right) = \frac{\alpha}{\|\mathbf{x}(k)\|_2^2 + \beta(k)}, \tag{12}$$

$$\mathbf{g}(k+1) = \mathbf{g}(k) + \eta(k)e(k)\mathbf{x}(k), \tag{13}$$

where $\mathbf{x}(k)$ and $\mathbf{g}(k)$ denote the vectors of input and tap weights at time index k respectively, α is the step-size parameter, and ρ is the offset learning rate parameter. The merit of the GNGD algorithm lies in the adaptation of its learning rate provides compensation for the assumptions in the derivation of normalized least mean squares (NLMS). Due to its robustness and stability, the GNGD is well-suited for narrowband nonstationary signal environments.

2.2.2 Analytic Signal and Hilbert Transform

For a one-dimensional real-valued signal $s(t) : \mathbb{R} \to \mathbb{R}$, we associate with it an complex-valued signal $z(t) = s(t) + jq(t)$, where the imaginary part $q(t)$ is defined via

$$q(t) = \mathcal{H}\left[s(t)\right] = s(t) * \frac{1}{\pi t} = \int_{\mathbb{R}} \frac{s(t-\xi)}{\pi\xi} d\xi. \tag{14}$$

Note that $q(t)$ is the Hilbert transform of $s(t)$, and the complex-valued signal $z(t)$ is called the analytic signal. Assume that $s(t)$ is a real-valued AM-FM signal given by

$$s(t) = a(t)\cos\left(\omega_c t + \phi(t)\right), \tag{15}$$

where $a(t)$ is the IA, ω_c is the carrier frequency and $\phi(t)$ is the phase for the IF $\phi'(t)$. Note that the IF defined here does not involve the carrier frequency ω_c. According to the basic property of the Hilbert transform and Bedrosian's theorem, $q(t)$ is the approximation to the product of the IA and the quadrature of the FM part as:

$$q(t) = \mathcal{H}\left[s(t)\right] \approx a(t) \sin\left(\omega_c t + \phi(t)\right). \tag{16}$$

However, this approximation is valid only if the following conditions hold:

1. $a(t)$ is a narrowband lowpass signal that varies slowly with time,
2. carrier frequency ω_c is sufficiently large such that

$$\omega_c \gg \phi'(t). \tag{17}$$

As a result, the corresponding analytic signal is of the form:

$$z(t) = s(t) + jq(t) \approx a(t) \exp\left[j\left(\omega_c t + \phi\left(t\right)\right)\right]. \tag{18}$$

Hence the IA $a(t)$ and the IF $\phi'(t)$ are estimated respectively by

$$a(t) \approx \|z(t)\|, \tag{19}$$

$$\phi'(t) \approx \frac{\partial}{\partial t}\left(\arctan\frac{\Im\left(z(t)\right)}{\Re\left(z(t)\right)}\right) - \omega_c. \tag{20}$$

2.2.3 Energy Separation Algorithm

The energy separation algorithm (ESA) as summarized in [2], based on the Teager-Kaiser energy operator, is widely used for monocomponent AM-FM demodulation. For a continous-time signal $x(t)$, the nonlinear Teager-Kaiser energy operator in the continuous case is given by

$$\Psi_c[x(t)] = \dot{x}^2(t) - x(t)\ddot{x}(t), \tag{21}$$

where $\dot{x}(t)$ and $\ddot{x}(t)$ denote the first and second derivatives of $x(t)$ respectively.

It was first introduced by Kaiser and was applied to track the energy of harmonic oscillation. For instance, the energy of the oscillatory signal $x(t) = A\cos(\omega_c t + \theta)$ can be tracked by the operator Ψ_c via

$$\Psi_c[A\cos(\omega_c t + \theta)] = (A\omega_c)^2. \tag{22}$$

The energy operator can be further used to analyze the oscillation of signals with time-varying amplitude and frequency. By applying the energy operators Ψ_c on the AM-FM signal, the IA $a(t)$ and IF $\omega_i(t)$ (excluding the carrier frequency ω_c) satisfy the following relation:

$$\Psi_c\left[a(t)\cos\left(\omega_c t + \int_0^t \omega_i(\tau)d\tau + \theta\right)\right] \approx \left[a(t)\left(\omega_c + \omega_i(t)\right)\right]^2. \tag{23}$$

As a result, the IA $a(t)$ and the IF $\omega_i(t)$ of an AM-FM signal $x(t)$ can be estimated via the continuous energy separation algorithm (CESA) summarized by

$$\frac{\Psi[x(t)]}{\sqrt{\Psi[\dot{x}(t)]}} \approx |a(t)|. \tag{24}$$

$$\sqrt{\frac{\Psi[\dot{x}(t)]}{\Psi[x(t)]}} - \omega_c \approx \omega_i(t), \tag{25}$$

where we assume that the IA $a(t)$ and the IF $\omega_i(t)$ do not vary too fast or too greatly in value compared to the carrier frequency ω_c.

2.3 Narrowband Constraint

Conventional demodulation techniques perform well only under the narrowband constraint. In general, the IA is required to be slowly-varying and the IF cannot change too fast or too greatly in value compared to the carrier frequency. To quantify the narrowband constraint, assume the IA $a(t)$ and the IF $\omega_i(t)$ are both bandlimited with highest frequencies ω_a and ω_f respectively. We further assume a nonnegative IA $a(t) = 1 + \kappa b(t)$ without loss of generality. The narrowband constraint can then be summarized similarly as in [2] via

$$\omega_a \ll \omega_c, \tag{26}$$

$$\kappa \ll 1, \tag{27}$$

$$\omega_f \ll \omega_c, \tag{28}$$

$$\lambda = \frac{\omega_m}{\omega_c} \ll 1, \tag{29}$$

where λ is the inverse of the CR/FD, which is also called the FM modulation depth. We can easily check that the narrowband constraint requires the two parameters CR/FD and CR/IB to be sufficiently large. However, it is not the case in the wideband scenario, where significant errors are incurred regardless of the choice of demodulation approaches. To improve the demodulation performance of existing approaches in the wideband scenario, we introduce the multirate frequency transformations (MFT) approach in the next section, that increases the CR/FD and CR/IB ratios for FM signals and for AM-FM signals also.

3 Methods, Assumptions, and Procedures

3.1 Wideband FM Demodulation Via Multirate Frequency Transformations

The MFT approach that involves multirate systems as well as heterodyning is proposed for wideband FM demodulation that usually has a: 1) large frequency deviation; 2) large information bandwidth. The proposed approach can be integrated with other existing FM demodulation methods, such as the analytic signal, negative feedback demodulation or energy operators, serving as a general framework for wideband FM demodulation.

3.1.1 Basic MFT System

Using the scaling property of the Fourier transform, compression in frequency domain is equivalent to expansion in the time domain expressed as

$$y(t) = x(at) \Longleftrightarrow Y(\omega) = X\left(\frac{\omega}{a}\right), \tag{30}$$

where $a = 1/R < 1$ is the factor of frequency compression. The IF of the compressed signal becomes a scaled version of the input IF by a factor R expressed as

$$\tilde{\omega}_i(t) = \frac{\omega_i(t)}{R} = \frac{\omega_c}{R} + \frac{\omega_m}{R} q_i\left(\frac{t}{R}\right). \tag{31}$$

Note that for a compressed signal, the carrier frequency is also scaled by the same factor R, which is undesirable since the ratios CR/FD and CR/IB that we wish to increase still remains invariant. Hence the heterodyning operator is cascaded right after the frequency compression module in order to upshift the carrier frequency to a higher level where we can attain larger CR/FD and CR/IB ratios. The compressed signal after frequency translation and bandpass filtering in the heterodyning module is given by

$$y_{ush}(t) = [y(t)\cos(\omega_d t)] * h_{BPF}(t), \tag{32}$$

where $*$ denotes the convolution, ω_d refers to the amount of frequency translation and $h_{BPF}(t)$ represents the impulse response of the bandpass filter. Specific for the case of sinusoidal FM, it can be further simplified as

$$y_{ush}(t) \simeq \frac{1}{2} A\cos\left(\phi\left(\frac{t}{R}\right)\right), \tag{33}$$

where $\phi(t)$ denotes the phase of the original FM signal. The resultant signal that has a scaled information bandwidth with a higher CR/IB then passes through the demodulation block for IF extraction. Eventually, the IF estimate of the original signal is evaluated by the inverse MFT relation via

$$\omega_i^{\text{out}}(t) = R\left(\tilde{\omega}_i(Rt) - \omega_d\right), \tag{34}$$

where $\tilde{\omega_i}(t)$ is the IF of the compressed and frequency translated signal.

As for a discrete-time signal, compression and expansion can be substituted by the corresponding multirate operations of interpolation and decimation respectively as described in [8] with their properties carried over to their discrete counterparts. The block diagram of the basic MFT framework in prior work [4] is illustrated by Fig. 1. The wideband signal is first sampled above the Nyquist rate, interpolated by a factor R and then heterodyned by multiplication with $\cos(\omega_d n)$, followed by a discrete Finite Impulse Response (FIR) bandpass filter with a scaling module based on (33) to achieve MFT. Then it goes through a demodulation block to obtain the IF estimation of the compressed heterodyned signal. To estimate IF of the original signal, the compressed heterodyned IF is then shifted back by subtracting ω_d, decimated by R and scaled back approapriately according to (31), followed by the DAC module.

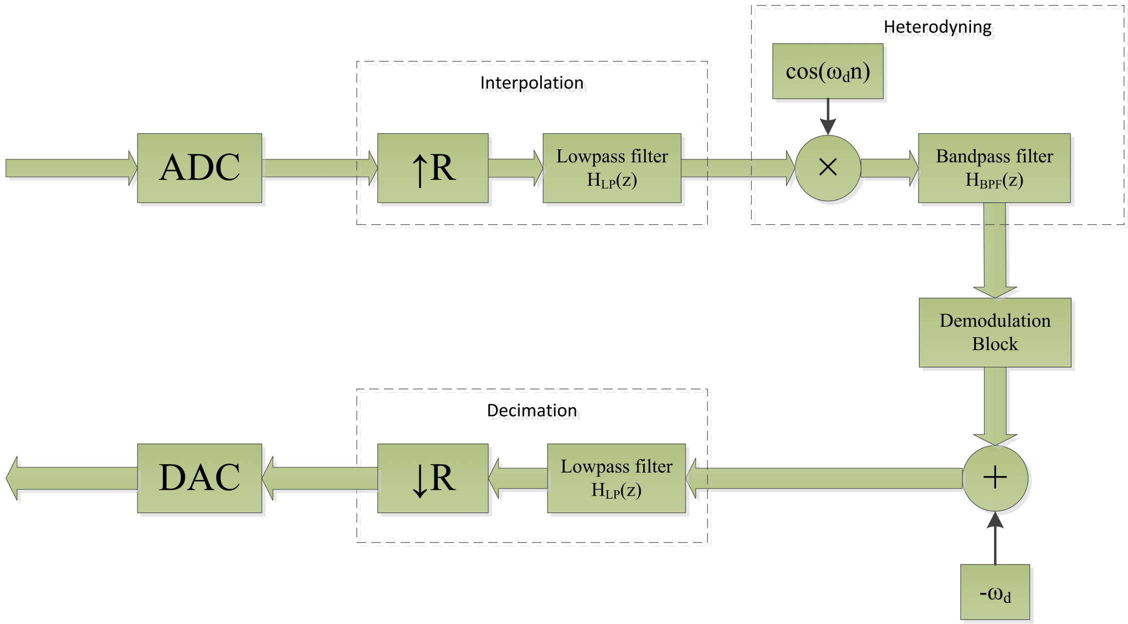

Figure 1: Block diagram of the basic MFT framework

Interpolating the input signal will result in the reduction of both the frequency deviation and information bandwidth by a factor of R. Similar to increasing the sampling rate, the IF of the interpolated signal becomes slow-varying and the assumption that the message signal remains constant over the carrier period is more likely to hold, which in turn boost the performances of conventional demodulation algorithms. Meanwhile, heterodyning serves the purpose of increasing the ratios of CR/FD and CR/IB by compensating for the scaled carrier frequency. By passing through the heterodyning process, the CR/FD and the CR/IB of $y_{ush}(t)$ are given by

$$\left[\frac{CR}{FD}\right]_{out} = \left[\frac{CR}{FD}\right]_{in} + \frac{R\omega_d}{\omega_m} \tag{35}$$

$$\left[\frac{CR}{IB}\right]_{out} = \left[\frac{CR}{IB}\right]_{in} + \frac{R\omega_d}{\omega_f}. \tag{36}$$

3.1.2 Error Analysis for Wideband FM Signals

Here we present the error analysis for wideband sinusoidal FM demodulation in 1D [1]. According to the handbook of mathematic formula and basic trigonometric identities, we have

$$\cos(\beta \sin\theta) = J_0(\beta) + 2\sum_{k=1}^{\infty} J_{2k}(\beta)\cos(2k\theta),$$

$$\sin(\beta \sin\theta) = 2\sum_{k=0}^{\infty} J_{2k+1}(\beta)\sin((2k+1)\theta)\,,$$

[1]The partial Hilbert transform is a separable combination of the 1D Hilbert transforms, consequently this analysis is valid for the proposed 2D approach as well.

$$\cos(u)\cos(v) = \frac{1}{2}[\cos(u-v) + cos(u+v)],$$
$$\sin(u)\sin(v) = \frac{1}{2}[\cos(u-v) - cos(u+v)],$$

where $J_n(\beta)$ denotes the Bessel function of the first kind.

Using above equations, the sinusoidal FM can be expanded as

$$\begin{aligned}
&\cos(\omega_c t + \beta\sin(\omega_m t)) \\
&= \cos(\omega_c t)\cos\left(\beta\sin(\omega_m t)\right) - \sin(\omega_c t)\sin\left(\beta\sin(\omega_m t)\right) \\
&= \cos(\omega_c t)J_0(\beta) + 2\sum_{k=1}^{\infty} J_{2k}(\beta)\cos(2k\omega_m t)\cos(\omega_c t) \\
&\quad - 2\sum_{k=0}^{\infty} J_{2k+1}\left(\beta\right)\sin((2k+1)\omega_m t)\sin(\omega_c t) \\
&= \cos(\omega_c t)J_0(\beta) + 2\sum_{k=1}^{\infty} J_{2k}(\beta)\cos\left((\omega_c + 2k\omega_m)t\right) \\
&\quad + 2\sum_{k=1}^{\infty} J_{2k}(\beta)\cos\left((\omega_c - 2k\omega_m)t\right) \\
&\quad + 2\sum_{k=0}^{\infty} J_{2k+1}(\beta)\cos\left((\omega_c t + (2k+1)\omega_m)t\right) \\
&\quad - 2\sum_{k=0}^{\infty} J_{2k+1}(\beta)\cos\left(\left(\omega_c - (2k+1)\omega_m\right)t\right)
\end{aligned}$$

Its quadrature part that we desire for demodulation can also be expanded similarly given by

$$\begin{aligned}
&\sin\left(\omega_c t + \beta\sin(\omega_m t)\right) \\
&= \sin(\omega_c t)\cos\left(\beta\sin(\omega_m t)\right) + \cos(\omega_c t)\sin\left(\beta\sin(\omega_m t)\right) \\
&= \sin(\omega_c t)J_0(\beta) + 2\sum_{k=1}^{\infty} J_{2k}(\beta)\cos(2k\omega_m t)\sin(\omega_c t) \\
&\quad + 2\sum_{k=0}^{\infty} J_{2k+1}\left(\beta\right)\sin((2k+1)\omega_m t)\cos(\omega_c t) \\
&= \sin(\omega_c t)J_0(\beta) + 2\sum_{k=1}^{\infty} J_{2k}(\beta)\sin\left((\omega_c + 2k\omega_m)t\right) \\
&\quad + 2\sum_{k=1}^{\infty} J_{2k}(\beta)\left(\sin(\omega_c - 2k\omega_m)t\right) + 2\sum_{k=0}^{\infty} J_{2k+1}(\beta)\sin\left(\left(\omega_c t + (2k+1)\omega_m\right)t\right) \\
&\quad - 2\sum_{k=0}^{\infty} J_{2k+1}(\beta)\sin\left(\left(\omega_c - (2k+1)\omega_m\right)t\right)
\end{aligned}$$

Note that the Hilbert transform of the corresponding sinusoidal FM can be easily obtained by performing the Hilbert transform at each of its harmonics as

$$
\begin{aligned}
&\mathcal{H}[\cos(\omega_c t + \beta \sin(\omega_m t))] \\
&= \sin(\omega_c t) J_0(\beta) + 2\sum_{k=1}^{\infty} J_{2k}(\beta) \sin(\omega_c + 2k\omega_m)t) \\
&\quad + 2\sum_{k=1}^{\infty} J_{2k}(\beta) \sin(|\omega_c - 2k\omega_m|t) \\
&\quad + 2\sum_{k=0}^{\infty} J_{2k+1}(\beta) \sin((\omega_c + (2k+1)\omega_m)\, t) \\
&\quad - 2\sum_{k=0}^{\infty} J_{2k+1}(\beta) \sin(|\omega_c - (2k+1)\omega_m|t)
\end{aligned}
$$

By comparing the quadrature and the Hilbert transform of the corresponding sinusoidal FM, we observe that when $\omega_c < n\omega_m$,

$$\mathcal{H}[\cos((\omega_c - n\omega_m)t)] = \sin(n\omega_m - \omega_c)t,$$

whereas the corresponding part in the quadrature part is of opposite sign $\sin(\omega_c - n\omega_m)t$. For narrowband sinusoidal FM, the Bessel coefficients $J_n(\beta)$ associated with these corresponding sidelobes are very small, and the demodulation error incurred by the Hilbert transform due to these opposite sign terms can be neglected. Hence the Hilbert transform, provides almost perfect reconstruction of the quadrature part we desire for demodulation using the analytic signal, for sinusoidal FM, in the narrowband case. For extremely wideband sinusoidal FM, however, due to its large modulation index β, the Bessel coefficients associated with these sidelobes cannot be neglected anymore. As a result, the error incurred by the Hilbert transform is much more significant. In general, this unavoidable error imposes a lower bound on the error performance for HT and energy operator in the extremely wideband scenario.

3.1.3 Alternative MFT System for Large Conversion Factors

As we look further into the MFT framework, an important question regarding the selection of the conversion factor R arises. Specifically prior work [4] only deals with small multirate compression factors. However, larger factors over hundred or thousand can be supported by current high-speed digital signal processing with large memory. It is intuitive to expect a further reduction in the demodulation error since the gain brought by frequency compression should be extendable through the use of a larger factor. But for sufficiently large factors R, the passband of the lowpass filter in the multirate operation and that of the heterodyne-band pass filter (BPF) operation will be scaled by R. For example, if $R = 1000$, we require a lowpass filter with cut-off frequency at $\pi/1000$ and a bandpass filter with a passband edge less than or equal to $\pi/1000$. However, filters with such narrow passbands are unrealistic for direct implementation by any structure[2]. Therefore, the

[2]Narrow passband implies clustered poles and zeros that result in sensitivity and stability issues of digital filters as described in [9].

design of the BPF within the basic MFT framework becomes the bottleneck that limits the use of a very large factor.

In general, the MFT framework achieves better demodulation performance when the conversion factor becomes larger. However, large conversion factors require the heterodyning bandpass filter to have significantly narrow passband, which is hardly achieved in practice. In order to reduce the burden placed on the practical implementation of the bandpass filter, we first consider a different MFT framework where the order of the interpolation operator and the heterodyning operator are exchanged. Due to the switch of interpolation and heterodyning, the CR/FD and CR/IB parameters under this MFT framework are given by

$$\left[\frac{CR}{FD}\right]_{out} = \left[\frac{CR}{FD}\right]_{in} + \frac{\omega_d}{\omega_m} \tag{37}$$

$$\left[\frac{CR}{IB}\right]_{out} = \left[\frac{CR}{IB}\right]_{in} + \frac{\omega_d}{\omega_f}. \tag{38}$$

By comparing these ratios with (35) and (36), note that the upshift frequency ω_d in this case needs to be sufficiently large such that the ratios of CR/FD and CR/IB still stay at high level. However, if ω_d is too large such that the resultant carrier frequency after heterodyning exceeds one half of the sampling rate, then we have to interpolate the signal first by an appropriate factor in order to perform discrete-time bandpass filtering after heterodyning. Hence the practical implementation of MFT framework for a large conversion factor is not as simple as just exchanging the order of interpolation and heterodyning. Actually, an interpolation operation is still required prior to the heterodyning with an appropriate factor that depends on the upshift frequency ω_d and the sampling frequency of the original wideband FM signal. This implies that the overall interpolation factor can be split into two with the first one prior to the frequency translation and the other one right after. Then upshifting by a frequency ω_d that is not too large would result in a relatively small factor for the first interpolation, thereby lessening the burden of the heterodyne-BPF.

In this section, we propose the alternative MFT framework for large conversion factor illustrated by Fig. 2(a) that achieves practical design of the heterodyne-BPF. Where Fig. 2(a) is the Block diagram of the proposed MFT framework for large wideband to narrowband conversion factors. The interpolation module of the prior framework is separated into two with one in front of the heterodyning module and the other one right after. The first interpolation module has a relatively small upsampling rate of R_1 which is appropriately chosen such that the discrete BPF can be implemented within the range of half the sampling rate after heterodyning the signal with a frequency translation of ω_d. The relatively small R_1 would result in a wider passband for the discrete bandpass filter, thus reducing the its design of complexity. And where Fig. 2(b) is the Multistage implementation for interpolation modules in Fig. 2(a) based on the Noble identity. Note that multistage implementation for the corresponding decimation modules can be realized in a similar fashion. As previously discussed, the interpolation module of the prior framework is separated into two with one in front of the heterodyning module and the other one right after in the proposed framework. The first interpolation module has a relatively small upsampling rate of R_1 which is appropriately chosen such that the discrete BPF can be implemented within the range of half the sampling rate after heterodyning the signal with a frequency translation of ω_d. The relatively small R_1 would result in a wider passband for the discrete bandpass filter, thus reducing complexity of the design. In general, there is a sacrifice in terms of achievable CR/IB and CR/FD

ratios for the alternative MFT framework. However, the basic MFT system cannot realize large conversion factors, due to the placement of impractical constraints on the BPF design.

In addition, a binomial smoothing module is incorporated into the alternative framework as shown in Fig. 2(a), to further reduce the effects of noise. Even though the FM signal is wideband, the IF waveform itself is not necessarily wideband in nature. In many cases, the wideband FM is primarily generated by a large modulation index while the IF waveform still remains in the narrowband range. Under this assumption, by applying the binomial smoothing we can efficiently filter out the high frequency noise in the corrupted IF estimation. When the signal to noise ratio (SNR) is high, the improvement becomes extremely evident as we shall see later. Usually we would expect a gain between 5 dB and 10 dB in the scenario of relatively high SNR.

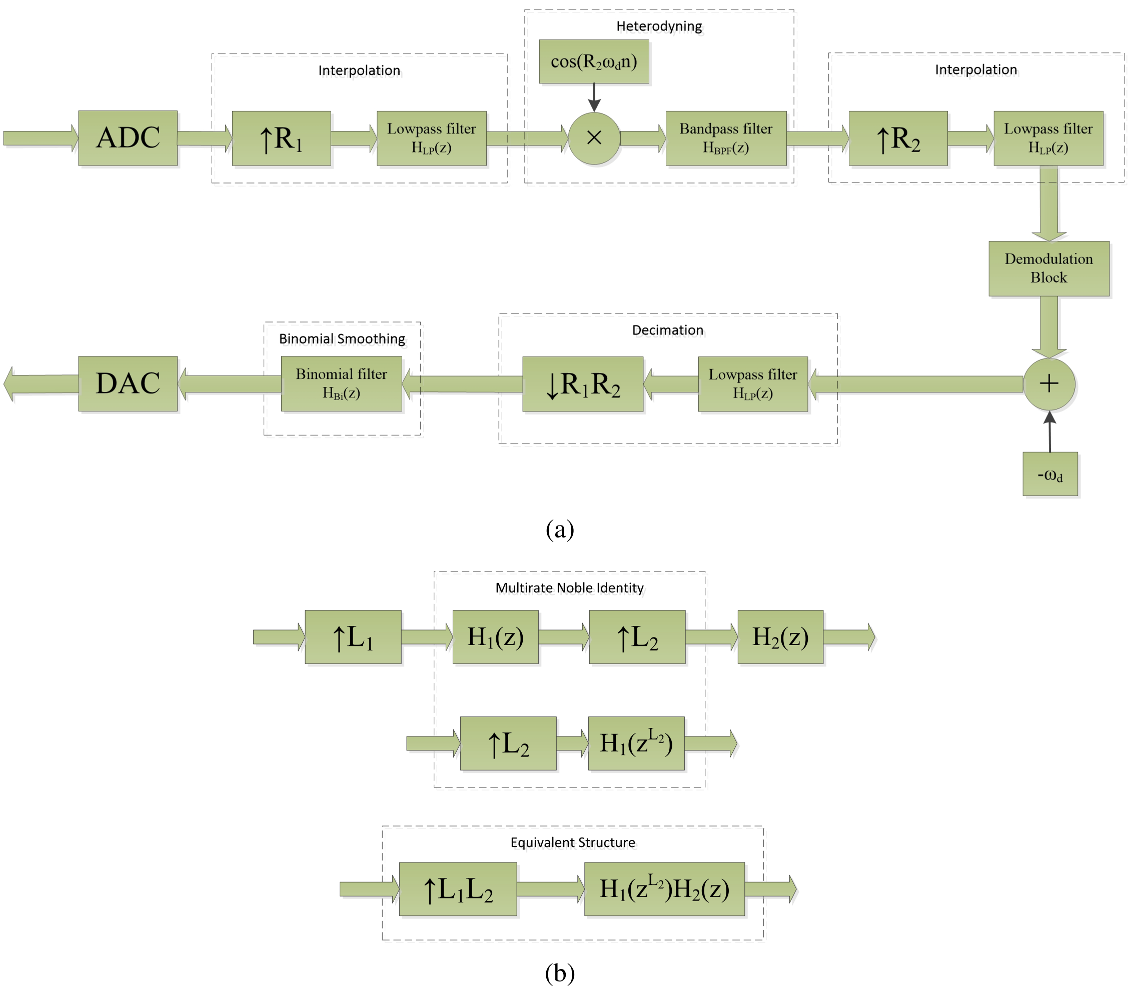

Figure 2: Block diagrams of the alternative MFT system for large conversion factors (a) and the Noble Identity relation (b) applied in the system.

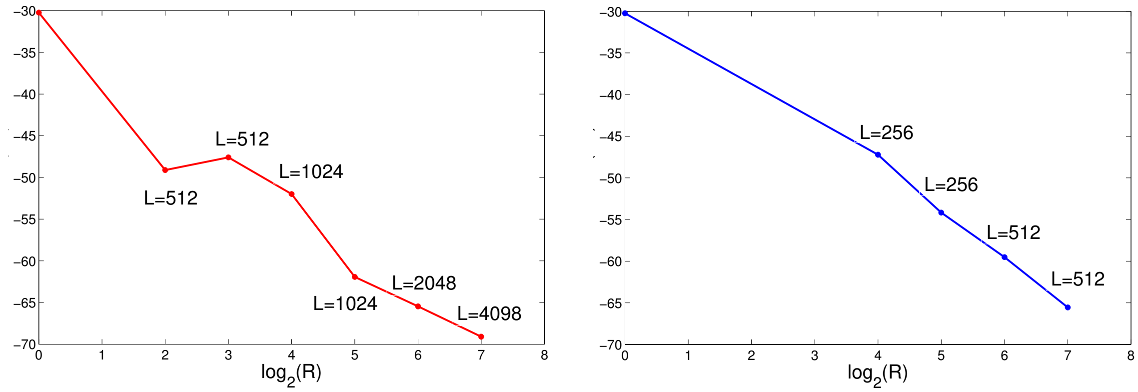

(a) (b)

Figure 3: Comparison between performances of both MFT frameworks under noise free environments. (a) Performance of the basic MFT framework. (b) Performance of the alternative MFT framework.

3.1.4 Examples of FM Demodulation via Both MFT Frameworks

In this section, we present demodulation results using the basic and alternative MFT frameworks respectively under both noise free and noisy environments. Here we apply the GNGD approach as the demodulation technique to test on pure FM signals. Note that the demodulation performance is judged by the normalized RMS IF demodulation error (NRMSE) throughout this section.

We first look at the case of a wideband sinusoidal FM signal that has a modulation index of 10 and the CR/IB of 20. Under a noise free environment, the performance of the basic MFT framework is illustrated by Fig. 3(a). Note that the performance associated with $R = 1$, i.e, the origin of the performance curve corresponds to direct demodulation by GNGD without MFT, while ω_d is the normalized upshift radian frequency translation in the range of $[0, \pi]$. By applying a large conversion factor of $R = 128$, a reduction of around 40 dB in the demodulation error over direct GNGD demodulation is attained. The result of Fig. 3(a) confirms the claim that a large conversion factor strengthens the benefits achieved by frequency compression thus leading to significant reduction in the demodulation error. Moreover, it reflects the fact that the use of a larger factor requires a very high order FIR bandpass filter with a satisfactory frequency response. For example, $R = 128$, demands the order of FIR bandpass filter to be as high as 4096, which results in unrealistic parameters for the narrow passband. This constraint seriously limits the implementation in a practical system for large factors.

To relax the constraint, the alternative MFT framework is applied, the demodulation performance of which is illustrated by 3(b). In comparison to Fig. 3(a), it can be observed that the required order for the FIR bandpass filter is effectively reduced at the cost of sacrificing a small amount of improvement in demodulation error. For instance, when $R = 128$, the order for the FIR bandpass filter drops significantly from 4096 to 512 with just 4 dB loss in performance, suggesting no observable difference in performance between both MFT frameworks except for the dramatic reduction of the order for the heterodyne-BPF. Note that the frequency response of the heterodyne-BPF in the alternative MFT framework for the case $R = 128$ is illustrated by Fig. 4(b), which has

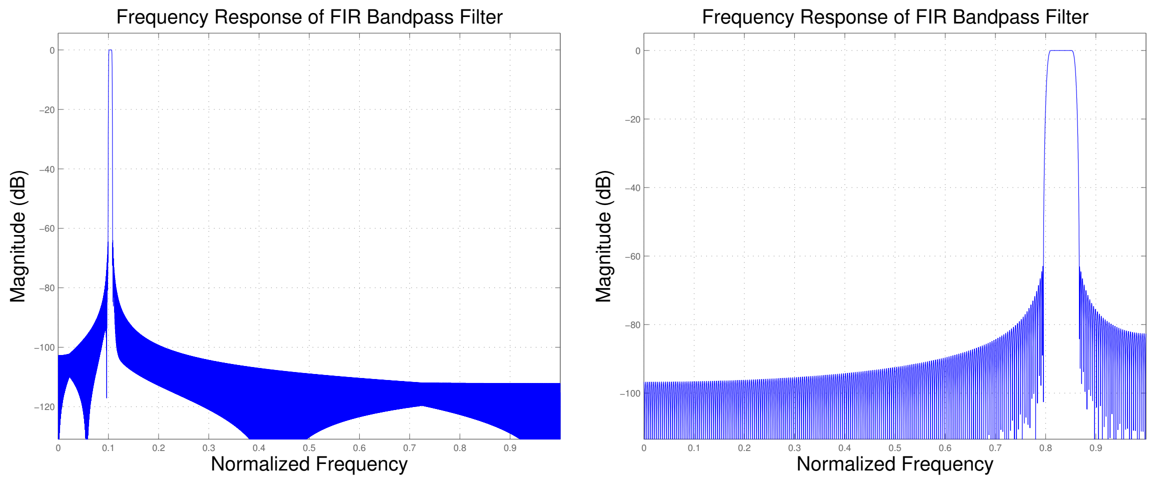

(a) (b)

Figure 4: Comparison between the basic and alternative MFT frameworks with a conversion factor $R = 128$. (a) Previous MFT framework. (b) Alternate MFT framework.

---

much wider passband compared to the frequency response of the BPF in the basic MFT framework shown in Fig. 4(a) and thus practical for implementation.

For noisy environments, the performance of the basic MFT framework is illustrated by Fig. 5(a) for the same sinusoidal FM signal corrupted by additive white Gaussian noise (AWGN). Based on this observation, improvement over GNGD demodulation alone varies according to the different SNRs. For example, when the SNR is 20 dB, the improvement is only aournd 6 dB, and when the SNR increases to 40 dB, improvement increases to around 20 dB. In addition, Fig. 5(b) summarizes the results of the alternative MFT framework in the presence of noise, indicating better performance due to the binomial smoothing. For the case of 20 dB SNR, the improvement increases to 15 dB compared with the basic MFT system. Note that the NRMSE gradually becomes saturated as R increases, due to LTI filtering induced harmonic distortion of the FM signals[3]. In contrast, the proposed MFT approach results in a better performance, and offers a more loose constraint on the BPF design.

We further investigate an extreme wideband scenario under the noise free environment, where the modulation index β is as large as 50 and the frequency deviation is equal to the carrier frequency with the IF varying over the entire carrier range. For the signal of interest, the IF estimates of both the basic and alternative MFT frameworks are illustrated by Fig. 6(a) and Fig. 6(b) respectively. It can be observed that the GNGD demodulation alone fails in this extreme wideband scenario, while both MFT frameworks maintain tracking. The observation implies that both MFT frameworks guarantee the demodulation with acceptable performance even in the worst scenarios where conventional algorithms would normally fail.

To quantify the performance of the MFT approach, we explore another scenario where the signal is a wideband linear chirp instead of a sinusoidal FM. The short-time spectrum of the chirp signal is illustrated by Fig. 7(a). To validate the performance of the MFT approach , we can compare

[3]Since they are only approximate eigenfunctions as described in [10].

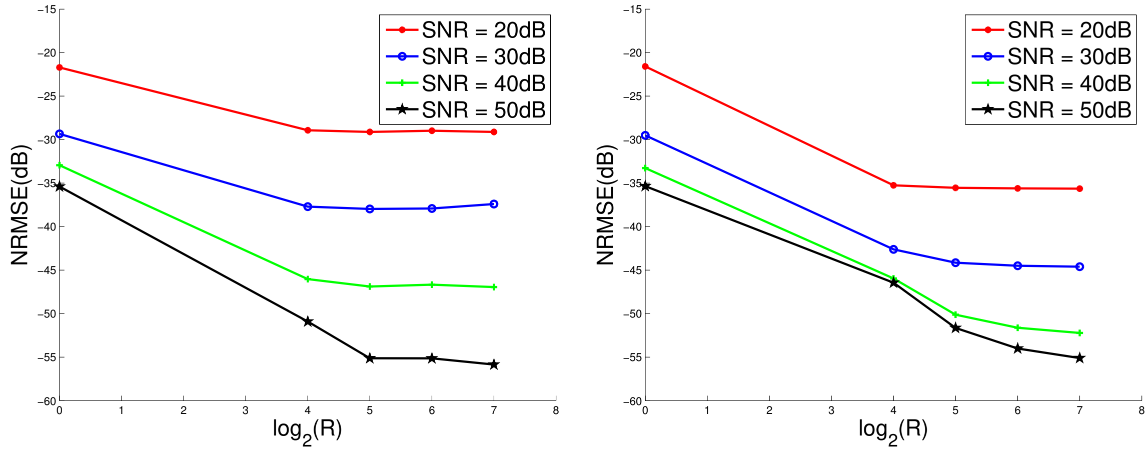

(a) (b)

Figure 5: Comparison between performances of both MFT frameworks in environments corrupted by AWGN. (a) The basic MFT framework. (b) The alternative MFT framework.

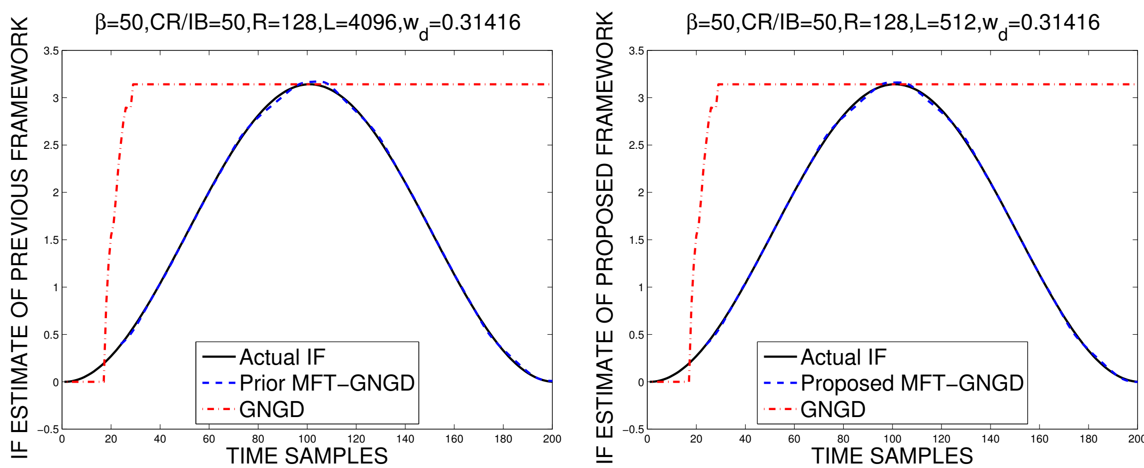

(a) (b)

Figure 6: Demodulation performances of both MFT frameworks with conversion factor $R = 128$ and normalized radian frequency shift $w_d = 0.1\pi$ under the extreme senario with modulation index $\beta = 50$.

the variance of error with respect to the chirp rate estimate with its *Cram´er Rao lower bound* (CRLB).

The chirp rate can be obtained from the demodulated IF followed by a least square estimator. In the presence of noise with different SNRs, the result is summarized in Fig. 7(b). Improvement over the GNGD alone is more apparent with respect to lower SNR, indicating satisfactory performance of the MFT approach in noisy conditions. Also note that gap between the error variance estimate of the MFT approach and the corresponding CRLB is nearly a constant, which can be explained directly via the loss of spectrum incurred due to filtering of the FM signal.

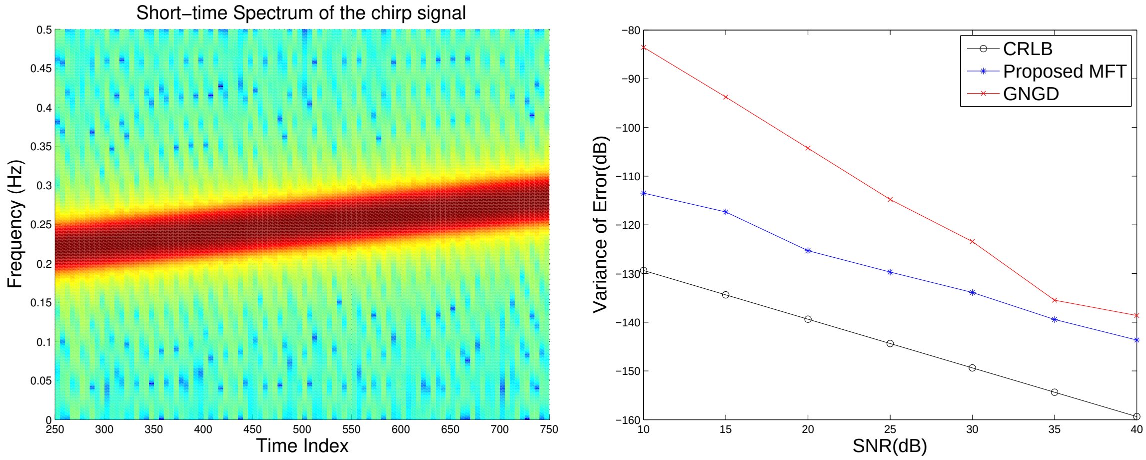

(a) (b)

Figure 7: Performance of the alternative MFT framework with a multirate conversion factor of 128 in wideband linear chirp scenario.

3.1.5 MFT Compatibility With HT And ESA Approaches

In general, the MFT framework can be combined with most demodulation approaches to enhance their performances in the wideband scenario. But the gain achieved by using the MFT framework varies with the demodulation algorithm employed. For a given demodulation scheme, the gain in error reduction via the Bi-directional multirate frequency transformation (BMFT) approach mainly depends on its inherent sensitivity to CR/IB, CR/FD, and the modulation index of the image. Here we refer to the comparison results of the HT approaches and ESA approaches in 1D [1].

The HT demodulation approaches are usually not very sensitive to the CR/IB of the signal. In general, the demodulation performance of the Hilbert transform is invariant to the CR/IB of the signal. As shown in the work [1] by Potamianos and Maragos, the error vesus CR/IB response of the Hilbert transform is almost flat, suggesting that by increasing the CR/IB via the MFT, the gain we achieve through error reduction is very limited. On the other hand, the ESA is shown to be very sensitive to the CR/IB of the signal, where the error decreases sharply as the CR/IB of the signal increases. Hence the gain attained by increasing the CR/IB via the MFT with demodulation schemes based on ESA is expected to be more significant than demodulation schemes using the HT approaches.

As for the CR/FD, both the HT and ESA demodulation methods suffer from large deviation compared with the carrier frequency. Hence the BMFT becomes beneficial to both of them via an increase in the CR/FD of the input.

Since the modulation index is jointly determined by both the CR/IB and CR/FD, its influence on the demodulation performance is not straightforward. However, the modulation index of the FM signal cannot be too large such that the spectrum of the sidelobes around the origin are significant and begin to incur significant demodulation error. The error incurred due to a large modulation index is unavoidable for any demodulation algorithm. It imposes a lower bound on the demodulation error. Even the MFT framework cannot reduce the error significantly in this extreme wideband scenario.

In conclusion, the proposed MFT approach is more suitable for the ESA demodulation schemes. Moreover, the MFT framework helps to overcome the estimation range constraint inherent in the ESA demodulation schemes. By compressing and shifting the original input in the frequency domain, we can always choose appropriate conversion factors and translation frequencies to convert its frequency components into the range between 0 and $\frac{\pi}{2}$. This is another advantage for combining the MFT framework with the ESA demodulation schemes.

In addition, the MFT framework can be extended in a straightforward separable way into multi-dimensional space and combined with the multi-dimensional higher order differential operators recently proposed by Salzenstein et al. [11]. Hence the analysis above also applies to the BMFT framework introduced in the next chapter.

4 Results and Discussions

4.1 Wideband Image Demodulation

The amplitude-modulation frequency-modulation (AM-FM) model has found various applications with images recently including image analysis, texture processing and fingerprint classification [12]. According to earlier work [13] by Havlicek, Bovik et al., nonstationary images can be modeled as superpositions of multiple AM-FM components,

$$I(x,y) = \sum_{i=1}^{n} a_i(x,y)\cos\left(\phi_i\left(x,y\right)\right). \tag{39}$$

The multi-component AM-FM image is first decomposed by employing a set of bandpass filters such as Gabor filterbanks or via the use of the Bi-dimensional Empirical Mode Decomposition (BEMD). Each resulting monocomponent AM-FM image is further demodulated into corresponding instantaneous amplitude (IA) $a(x,y)$ and instantaneous frequency vector (IF),

$$\nabla\phi(x,y) = \left[\frac{\partial\phi(x,y)}{\partial x}, \frac{\partial\phi(x,y)}{\partial y}\right]^T. \tag{40}$$

In particular, the IA depicts the contrast present in the image, while the IF reveals the locally emergent frequency variation. Conventional image demodulation approaches involve 2D extension of the analytic signal (AS) and multidimensional Energy Separation Algorithm (ESA) [14] with additional processing techniques such as Dominant Component Analysis (DCA). However, in most of these approaches, narrowband assumptions were imposed on each AM-FM component of the image. For example, most literature implicitly assumes the AM-FM image to be globally wideband yet each of its components to be locally narrowband. In general, both the IA, $a(x,y)$ and the IF, $\nabla\phi(x,y)$ of a single component are assumed to be slowly varying, otherwise the approximations inherent in most demodulation approaches are no longer valid and incur significant error especially under the wideband scenario.

In this chapter, we propose the 2D extension of the MFT approach called the Bi-dimensional Multirate Frequency Transformations (BMFT) that can be combined with a variety of demodulation techniques to enhance the demodulation performance, traditionally limited by the narrowband constraint on the frequency modulation part of the monocomponent AM-FM image.

4.1.1 Wideband Frequency Modulated Image

Since images are not separable in general, we cannot directly extend the related definitions of 1D wideband signal to 2D. For instance, we are not able to define the corresponding modulation index along any specific direction for 2D images in a global sense. However, as proposed by Pattichis and Bovik [15], the complex FM image can be locally approximated by the product of two 1D FM signals. The corresponding 1D signals are defined along the directions of the eigenvectors of the instantaneous frequency gradient tensor (IFGT), which is simply the Hessian of the phase. Let $\vec{z} = [z_1, z_2]$ denote the representation under the eigenvector coordinate system, $\widetilde{\phi}(\vec{z})$ denote the phase of the FM image and $\widetilde{\vec{F}}$ denote the IFGT. According to [15], around a given point

$\vec{z}_0 = [a_1, a_2]$ of the image, the local phase is approximated using a Taylor series expansion by

$$\widetilde{\phi}(\vec{z}) \approx \widetilde{\phi}(a_1, a_2) + \widetilde{\phi}_1(z_1) + \widetilde{\phi}_2(z_2), \tag{41}$$

where:

$$\widetilde{\phi}_i(z_i) = \frac{\partial \widetilde{\phi}}{\partial z_i}(a_1, a_2)(z_i - a_i) + \frac{\lambda_i(a_1, a_2)}{2}(z_i - a_i)^2,\ i = 1, 2. \tag{42}$$

Note that λ_1 and λ_2 are the eigenvalues of $\widetilde{\vec{F}}$. The complex FM image is then locally approximated by the product of two 1D FM functions defined with respect to the eigenvector coordinate directions:

$$\exp\left[j\widetilde{\phi}(z_1, z_2)\right] \approx \exp\left[j\phi_1(z_1)\right] \exp\left[j\phi_2(z_2)\right]. \tag{43}$$

As a result, FM images can be viewed as locally separable, and we can define the wideband FM images locally by deriving the corresponding parameters along the eigenvector coordinate directions. For example, if the modulation index along the directions of the IFGT eigenvectors are sufficiently large around the reference point, the image can be expected to exhibit similar wideband pattern locally analogous to the 1D case. Assume the modulation index along both directions of the eigenvectors are denoted by β_{z_1} and β_{z_2} respectively. To locally indicate whether an FM image is wideband or not in the sense similar to the literature in FM communication systems, we can define a local modulation index β_l via

$$\beta_l = \left(\beta_{z_1}^2 + \beta_{z_2}^2\right)^{1/2}. \tag{44}$$

If β_l is sufficiently large, then the corresponding FM image exhibits a wideband pattern locally. This definition of the local modulation index β_l is especially effective for the sinusoidal FM images with IF components specified along the horizontal and vertical directions. In this case, the modulation index for each eigenvector direction can be well defined according to the original formulation in the 1D context.

4.1.2 Partial Hilbert Transform Demodulation

The partial or directional Hilbert transform based on analytic image is widely used for monocomponent AM-FM image demodulation.

It can be derived simply from the 1D Hilbert transform. Let $f(\vec{x}) : \mathbb{R}^n \to \mathbb{R}$ and $\vec{e}_i$ denote the unit vector in the x_i direction. The partial Hilbert transform along the direction of $\vec{e}_i$ is then defined by

$$\mathcal{H}_{x_i}\left[f(\vec{x})\right] = \int_{\mathbb{R}} \frac{f(\vec{x} - \xi\vec{e}_i)}{\pi\xi} d\xi. \tag{45}$$

Note that the partial Hilbert transform defined here is specified along the horizontal and vertical directions. Thus it is particularly suitable for demodulating images with frequency modulation patterns emerging along the same directions. Assume that $I(x, y)$ is a monocomponent AM-FM image with frequency modulation patterns emerging along both the horizontal and vertical directions given by

$$I(x, y) = A(x, y)\cos\left(\Omega_x x + \Omega_y y + \varphi(x, y)\right), \tag{46}$$

where Ω_x and Ω_y denote the carrier (mean) frequencies along the x and y directions respectively. Under this assumption, analogous to the one dimensional problem, we are able to approximate the partial Hilbert transform along the x axis by fixing variable y via

$$\mathcal{H}_x\left[I(x,y)\right] \approx A(x,y)\sin\left(\Omega_x x + (\Omega_y y + \varphi(x,y))\right). \tag{47}$$

This approximation holds only under certain conditions similar to the 1D case. First of all, the $A(x,y)$ should be slow-varying and narrowband. Analogous to the one dimensional narrowband constraint, Ω_x is required to be sufficiently large such that

$$\Omega_x \gg \frac{\partial\varphi(x,y)}{\partial x}. \tag{48}$$

A similar condition applies to the y axis as well. As a result, we can easily obtain the approximations for the IA and the IF components with respect to both directions according to the 2D extensions of the corresponding one dimensional IA and IF estimates.

Synthetic examples are provided to illustrate the efficacy of the proposed approach. Since the synthetic images we present are predefined with its frequency modulation patterns along horizontal and vertical directions, the partial Hilbert transform is preferred over the monogenic image approach to serve as the comparison technique to the proposed approach due to the following reasons: 1) the demodulation performance of the partial Hilbert transform is as competitive as the Riez transform when the image display frequency modulation patterns along the same specified directions, 2) the partial Hilbert transform can be implemented easily via the 1D Hilbert transform.

4.1.3 Higher Order Energy Operator

A variety of methods based on the multidimensional energy operator [14] are also widely used for AM-FM image demodulation. An image demodulation algorithm based on higher order Teager-Kaiser operators is proposed in the recent work [16] by Salzenstein, Diop and Boudraa. They have been reported to provide better performance for narrowband AM-FM images than the classical 2D ESA [14].

The k-order differential energy operator (DEO) [20] in 1D for any given signal $s(t)$ is defined by

$$\Psi_k[s(t)] = \frac{\partial s(t)}{\partial t}\frac{\partial^{k-1}s(t)}{\partial t^{k-1}} - s(t)\frac{\partial^k s(t)}{\partial t^k}, \tag{49}$$

where Ψ_2 refers to the commonly used Teager-Kaiser energy operator. For a given image $I(k,l)$, the discrete-time higher order demodulation algorithm (DHODA) [16] can be summarized via:

$$I_1(k,l) = \frac{1}{2}[I(k+1,l) - I(k-1,l)], \tag{50}$$

$$I_2(k,l) = \frac{1}{2}[I(k,l+1) - I(k,l-1)], \tag{51}$$

$$I_{12}(k,l) = \frac{1}{2}[I_2(k+1,l) - I_2(k-1,l)], \tag{52}$$

$$\begin{aligned}\Psi_2[I(k,l)] =& \{2[I(k,l)]^2 - I(k-1,l)I(k+1,l) - I(k,l-1)I(k,l+1)\} \\ &+ 2[I_1(k,l)I_2(k,l) - I(k,l)I_{12}(k,l)],\end{aligned} \tag{53}$$

$$I_{12}^1(k,l) = \frac{1}{2}[I_{12}(k+1,l) - I_{12}(k-1,l)], \tag{54}$$

$$I_{12}^2(k,l) = \frac{1}{2}[I_{12}(k,l+1) - I_{12}(k,l-1)], \tag{55}$$

$$|\widehat{a}(k,l)| = \left(\frac{\Psi_2[I_1(k,l)]\Psi_2[I_2(k,l)]}{\Psi_2[I_{12}^1(k,l) + I_{12}^2(k,l)]}\right)^{1/2}, \tag{56}$$

$$|\widehat{\Omega}_1(k,l)| = \arcsin\left(\left(\frac{\Psi_2[I_{12}(k,l)]}{\Psi_2[I_2(k,l)]}\right)^{1/2}\right), \tag{57}$$

$$|\widehat{\Omega}_2(k,l)| = \arcsin\left(\left(\frac{\Psi_2[I_{12}(k,l)]}{\Psi_2[I_1(k,l)]}\right)^{1/2}\right), \tag{58}$$

where $\widehat{a}(k,l)$ is the IA estimation while $\widehat{\Omega}_1(k,l)$ and $\widehat{\Omega}_2(k,l)$ are the IF estimations along the spatial axes of the image. Note that the IF estimations are obtained through the inverse sine function, indicating that the demodulation approaches based on the ESA can only estimate IF components that range between 0 and $\frac{\pi}{2}$, or in other words, up to one fourth of the sampling frequency. Moreover, the demodulation approaches based on the ESA also suffer from the narrowband constraint as the Hilbert transform. Both the IA and the IF waveforms may not vary too fast or too greatly in value.

4.1.4 Bi-dimensional Multirate Frequency Transformations

The Multirate Frequency Transformations (MFT) approach that performs wideband to narrowband conversion of a FM signal was proposed in the previous section. The MFT primarily increases the CR/IB and CR/FD ratios of the original signal to improve the demodulation performance of the conventional demodulation approaches. The corresponding Bi-dimensional Multirate Frequency Transformation (BMFT) is derived by generalizing the underlying idea to 2D. For simplicity, assume that the input is a monocomponent wideband FM image of the form

$$J(x,y) = A\cos\left(\phi(x,y)\right). \tag{59}$$

It is first compressed in frequency domain by appropriate factors $\vec{R} = \mathrm{diag}[R_x, R_y]$, which corresponds to spatial expansion given by

$$J_1(x,y) = A\cos\left(\phi\left(\frac{x}{R_x}, \frac{y}{R_y}\right)\right). \tag{60}$$

Then we heterodyne the resultant image by a frequency translation vector $\vec{\Omega} = [\Omega_x, \Omega_y]$ via

$$
\begin{aligned}
J_2(x,y) =& J_1(x,y)\cos(\Omega_x x)\cos(\Omega_y y) \\
=& \frac{A}{2}\cos\left(\Omega_x x + \phi\left(\frac{x}{R_x}, \frac{y}{R_y}\right)\right)\cos(\Omega_y y) \\
&+ \frac{A}{2}\cos\left(\Omega_x x - \phi\left(\frac{x}{R_x}, \frac{y}{R_y}\right)\right)\cos(\Omega_y y) \\
=& \frac{A}{4}\cos\left(\Omega_x x + \Omega_y y + \phi\left(\frac{x}{R_x}, \frac{y}{R_y}\right)\right) \\
&+ \frac{A}{4}\cos\left(\Omega_x x - \Omega_y y + \phi\left(\frac{x}{R_x}, \frac{y}{R_y}\right)\right) \\
&+ \frac{A}{4}\cos\left(\Omega_x x + \Omega_y y - \phi\left(\frac{x}{R_x}, \frac{y}{R_y}\right)\right) \\
&+ \frac{A}{4}\cos\left(\Omega_x x - \Omega_y y - \phi\left(\frac{x}{R_x}, \frac{y}{R_y}\right)\right).
\end{aligned} \tag{61}
$$

After the heterodyning a 2D bandpass filter is applied to extract the desired high-frequency term through

$$
\begin{aligned}
\widetilde{J}(x,y) &= J_2(x,y) * h_{BP}(x,y) \\
&\approx \frac{A}{4}\cos\left(\Omega_x x + \Omega_y y + \phi\left(\frac{x}{R_x}, \frac{y}{R_y}\right)\right) \\
&= \frac{A}{4}\cos\left(\widetilde{\phi}(x,y)\right).
\end{aligned} \tag{62}
$$

Assume that the support of the original image spectrum $J(\omega_1, \omega_2)$ is within the range $\omega_i \in [-\Omega_i, \Omega_i],\ i = 1, 2$. The 2D bandpass filter should be carefully designed with its passband range given by

$$
|\omega_1| \in [\Omega_x, \Omega_x + \frac{\Omega_1}{R_x}],\ |\omega_2| \in [\Omega_y, \Omega_y + \frac{\Omega_2}{R_y}]. \tag{63}
$$

On one hand, the carrier (or mean) frequencies of the modulation in both dimensions are increased via the frequency translation vector $\vec{\Omega} = [\Omega_x, \Omega_y]$. On the other hand, the bandwidth of the modulating image is reduced by the appropriate conversion factors $\vec{R} = \mathrm{diag}[R_x, R_y]$. These two benefits derived via the BMFT are crucial to improving IF demodulation due to the following reasons: 1) a majority of demodulation approaches require the input to have high CR/IB in both dimensions, 2) the CR/FD of the input must be sufficiently large in both dimensions such that the deviations of the IF components can be tolerated in accordance with the narrowband assumption of the input.

Then we can recover the IF of the input image from the IF estimation of the transformed image $\widetilde{J}(x,y)$ via the inverse BMFT. Assume that the IF components of $J_(x,y)$ and $\widetilde{J}(x,y)$ are given by

$$
\Omega_1(x,y) = \frac{\partial\phi(x,y)}{\partial x}, \quad \Omega_2(x,y) = \frac{\partial\phi(x,y)}{\partial y}, \tag{64}
$$

$$\widetilde{\Omega}_1(x,y) = \frac{\partial\widetilde{\phi}(x,y)}{\partial x}, \quad \widetilde{\Omega}_2(x,y) = \frac{\partial\widetilde{\phi}(x,y)}{\partial y}. \tag{65}$$

The IF estimation for input image is recovered through the inverse BMFT relation (see Fig. 8) via

$$\Omega_1(x,y) = R_x\left(\widetilde{\Omega}_1(R_x x, R_y y) - \Omega_x\right), \tag{66}$$

$$\Omega_2(x,y) = R_y\left(\widetilde{\Omega}_2(R_x x, R_y y) - \Omega_y\right), \tag{67}$$

where $\widetilde{\Omega}_1(R_x x, R_y y)$ and $\widetilde{\Omega}_2(R_x x, R_y y)$ represent spatial compression (or frequency expansion) of the IF estimation for the transformed image $\widetilde{J}(x,y)$.

In order to implement the BMFT in discrete time, we replace compression and expansion in frequency domain by their discrete equivalences. Note that the compression in the frequency domain corresponds to interpolation while the expansion corresponds to decimation. As a result, the block diagram of the BMFT demodulation approach is depicted in Fig 8. The BMFT is implemented through discrete-time operations of interpolation, heterodyning, and bandpass filtering. The transformed FM image is then demodulated via a monocomponent demodulation approach and the original IF components are recovered from the IF estimation of the transformed image via the inverse BMFT. However, discrete-time operations in 2D may not be extended in a straightforward way from their 1D counterpart. It primarily depends on whether the input image is separable or not. If the image is separable, each operation of the BMFT can be implemented by simply cascading its 1D equivalence with action along each dimension. If this is not the case, we need to pay attention to a few issues associated with the non-separable nature of the image, which are often intractable. Therefore, deriving 2D operations directly from their 1D realizations is favored in terms of its simplicity for practical implementation.

In particular, the frequency upshift in heterodyning is not uniquely defined in 2D. This can be realized either through the product of two separable cosine terms $\cos(\Omega_1 m)\cos(\Omega_2 n)$ in each dimension as in Fig. 8 or via just one cosine term $\cos(\Omega_1 m + \Omega_2 n)$ in the diagonal direction. These two different realizations will lead to different designs of the 2D bandpass filters. For the first case, we only need to bandpass the outermost quarter of the frequency spectrum in each quadrant to extract the desired high frequency term expressed in (62). This is simply achieved using a separable 2D bandpass filter, by cascading two 1D bandpass filters with action in each dimension. For the latter case, where the frequency upshift is diagonal, it is much more complicated to achieve the same objective with a realizable design of the 2D bandpass filter. The issue is that the 2D frequency upshift in the diagonal direction results in only two copies of the original spectrum in the first and third quadrant respectively. However, the design of a 2D bandpass filter whose passband is only present in two quadrants and also capable of extracting the desired term in (62) is computationally complex.

In addition, the BMFT framework can be directly applied on a monocomponent AM-FM image provided that the IA of the given image is slowly varying, which is inherently assumed by most image demodulation algorithms. Under this constraint, the IA can be approximated via the inverse BMFT relation by

$$A(x,y) = \widetilde{A}\left(R_x x, R_y y\right), \tag{68}$$

where $\widetilde{A}\left(x,y\right)$ denotes the demodulated IA of the transformed image $\widetilde{J}(x,y)$. Numerical results are given later in this chapter to support this claim.

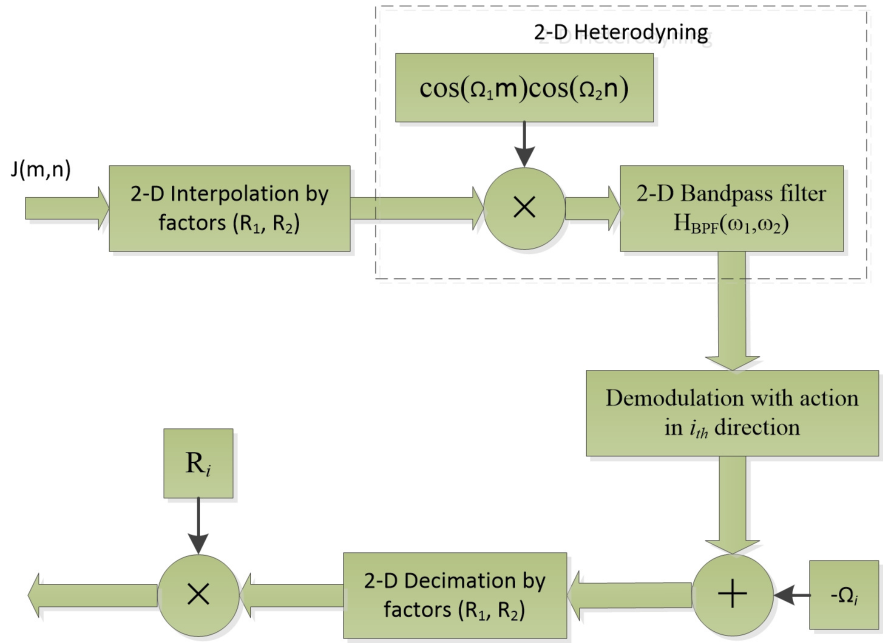

Figure 8: Block diagram of the Bi-dimensional Multirate Frequency Transformations (BMFT).

4.1.5 Example of Wideband Image Demodulation

In this section, we present numerical results for the proposed BMFT-energy approach. We begin with an example of a synthetic sinusoidal AM-FM image as illustrated in Fig. 9. The expression of this synthetic image and its corresponding IF components are given by

$$\begin{aligned} f(m,n) = &\left[1 + 0.5\cos\left(\frac{\pi}{50}m + \frac{\pi}{30}n\right)\right]\cos(\frac{\pi}{5}m + \frac{\pi}{3}n + 6\sin\left(\frac{\pi}{50}m + \frac{\pi}{2}\right) + \\ &5\sin\left(\frac{\pi}{30}n\right)), \end{aligned} \tag{69}$$

$$\Omega_1(m,n) = \frac{\partial\phi(m,n)}{\partial m} = \frac{\pi}{5} + \frac{3\pi}{25}\cos\left(\frac{\pi}{50}m + \frac{\pi}{2}\right), \tag{70}$$

$$\Omega_2(m,n) = \frac{\partial\phi(m,n)}{\partial n} = \frac{\pi}{3} + \frac{\pi}{6}\cos\left(\frac{\pi}{30}n\right). \tag{71}$$

Note that the frequency modulation index is 6 along the horizontal direction and 5 along the vertical direction, both of which are sufficiently large. We can also easily check that the CR/IB and the CR/FD are small along both directions for this wideband sinusoidal example.

The demodulation results via the DHODA combined with the proposed BMFT framework using conversion factors of $\vec{R} = \mathrm{diag}[8,8]$ are given by Fig. 10. Specifically, Fig. 10 represents the perspective plot of the demodulation results for the wideband sinusoidal example via the DHODA and via the BMFT-DHODA with conversion factors $\vec{R} = \mathrm{diag}[8,8]$. Fig. 10(a) is the estimation of the IA via the DHODA. Fig. 10(b) is the estimation of the IA via the BMFT-DHODA. Fig. 10(c) is the estimation of the IF component along the horizontal direction via the DHODA. Fig. 10(d) is the estimation of the IF component along the vertical direction via the DHODA. Fig. 10(e) is

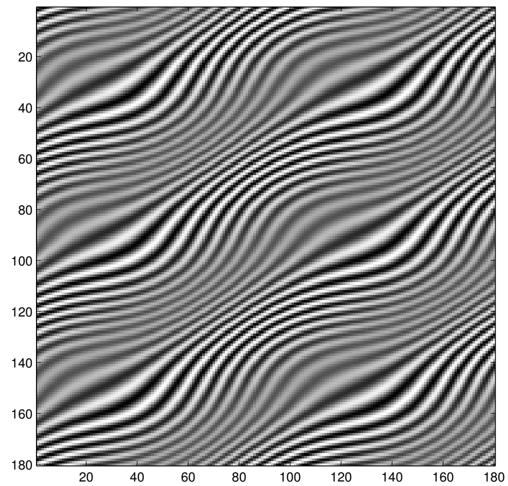

Figure 9: Synthetic sinusoidal AM-FM image with wideband FM components.

the estimation of the IF component along the horizontal direction via the BMFT-DHODA. Finally, Fig. (f) 10(f) is the estimation of the IF component along the vertical direction via the BMFT-DHODA. It is compared with the demodulation via the DHODA alone. Note that the demodulated IF with respect to either the horizontal or the vertical direction exhibits a sinusoidal pattern along that direction, which can be inferred from (69). We can easily observe that both the IA and the IF obtained via the BMFT-DHODA are smoother than that via the DHODA alone. The MSE for the IA is reduced from 0.8910 to 0.0649 and the root mean square error (RMSE) for the IF is reduced significantly from 1.83% to 0.25% through the BMFT framework. Here we define the RMSE as the l_2 norm of the difference between the true IF, $\nabla\phi(x,y)$ and the estimated IF, $\nabla\widehat{\phi}(x,y)$ against the l_2 norm of the true IF itself via

$$\text{RMSE} = \frac{\|\nabla\phi(x,y) - \nabla\widehat{\phi}(x,y)\|_{l_2}}{\|\nabla\phi(x,y)\|_{l_2}} \times 100\%. \tag{72}$$

In fact, the demodulation error can be further reduced if larger multirate conversion factors are applied, similar to the 1D case of MFT. As shown in Table 1, the demodulation errors of the proposed BMFT framework using DHODA with conversion factors of $\vec{R} = \mathrm{diag}[8,8]$ (BMFT-DHODA-8) and with conversion factors of $\vec{R} = \mathrm{diag}[16,16]$ (BMFT-DHODA-16) are compared with the DHODA alone. The RMSE can be further reduced to 0.18% via the BMFT with conversion factors $\vec{R} = \mathrm{diag}[16.16]$, achieving an error reduction of 10 times compared with the DHODA alone. The use of larger factors results in a much narrower passband for digital filters that are difficult to realize in practice due to a sharper transition band. To implement such FIR filters, a very large filter order is required, which may not be acceptable in terms of the desired system complexity. Therefore the choice of multirate conversion factors should be weighted between the tolerance for demodulation error and that of the system complexity. Recently the BMFT structure using large conversion factors has been implemented via an equivalent structure that alleviates the complexity of practical realization. Aided by this equivalent structure, we may further reduce the demodulation error by exploring even larger conversion factors.

The demodulation results via the partial Hilbert transform alone (HTDA) and the BMFT and

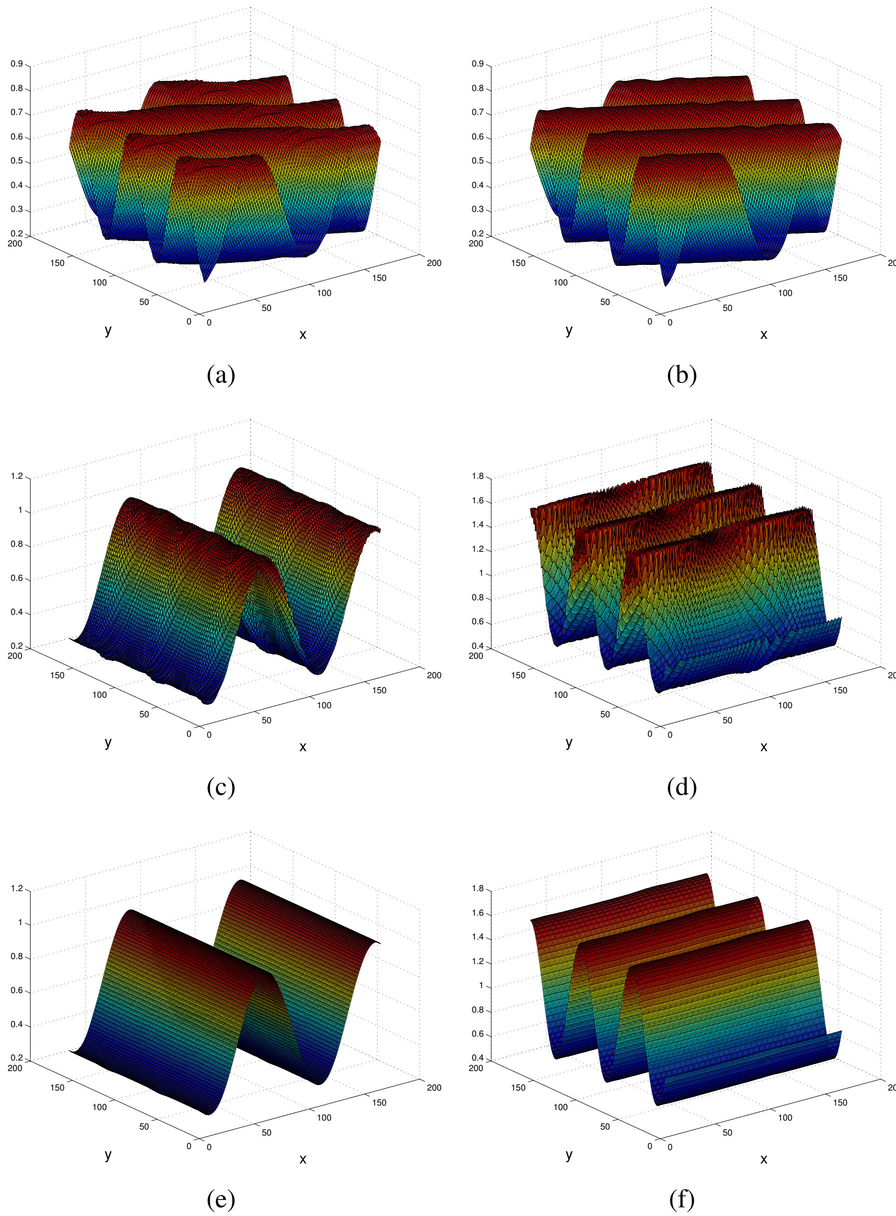

Figure 10: Perspective plot of the demodulation results for the wideband sinusoidal example via the DHODA and via the BMFT-DHODA

the partial Hilbert transform combination with conversion factors $\vec{R} = \mathrm{diag}[8, 8]$ (BMFT-HTDA-8) are also illustrated in Table 1. We can observe that the error reduction via the BMFT framework for the HT demodulation is not as obvious as for the ESA demodulation, which justifies our discussion in the previous section.

In the second experiment, we test the BMFT and the DHODA combination on a wideband sinusoidal FM image whose IF components are out of the range $[0, \frac{\pi}{2}]$, which is the estimation range constraint for demodulation approaches based on the ESA. As shown in Fig. 11, the synthetic

Table 1: Comparison of the demodulation errors

	$\mathrm{var}(\frac{a-\widehat{a}}{a})$	$\mathrm{MSE}(a,\widehat{a})$	$\mathrm{var}(\frac{\Omega_1-\widehat{\Omega}_1}{\Omega_1})$	$\mathrm{var}(\frac{\Omega_2-\widehat{\Omega}_2}{\Omega_2})$
DHODA	4.7876	0.8910	2.6688	8.0073%
BMFT-DHODA-8	0.2934	0.0649	0.3554	0.1281%
BMFT-DHODA-16	0.1677	0.0412	0.5608	0.0813%
HTDA	0.5125	0.0942	0.3715	0.0683%
BMFT-HTDA-8	0.2930	0.0646	0.1228	0.0796%
	$\mathrm{MSE}(\Omega_1,\widehat{\Omega}_1)$	$\mathrm{MSE}(\Omega_2,\widehat{\Omega}_2)$	RMSE	
DHODA	0.6948	12.9626	1.83%	
BMFT-DHODA-8	0.0427	0.1310	0.25%	
BMFT-DHODA-16	0.0419	0.0701	0.18%	
HTDA	0.1276	0.0430	0.23%	
BMFT-HTDA-8	0.0235	0.0716	0.20%	

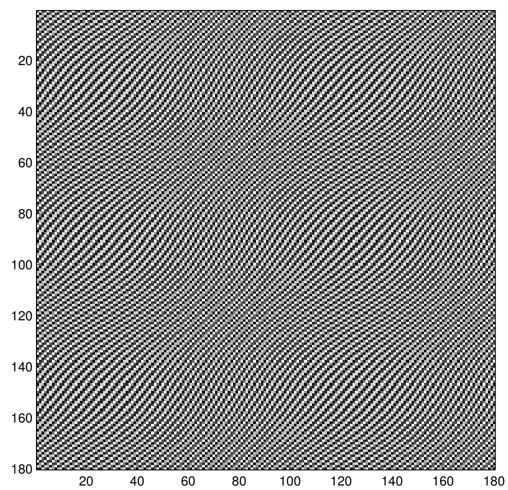

Figure 11: Wideband sinusoidal FM image with IF components outside the range of ESA constraint

image for this example and its corresponding IF components are given by:

$$f(m,n) = 0.5\cos(\frac{2\pi}{3}m + \frac{2\pi}{3}n + 6\sin\left(\frac{\pi}{50}m + \frac{\pi}{2}\right) + 5\sin\left(\frac{\pi}{30}n\right)), \tag{73}$$

$$\Omega_1(m,n) = \frac{\partial\phi(m,n)}{\partial m} = \frac{2\pi}{3} + \frac{3\pi}{25}\cos\left(\frac{\pi}{50}m + \frac{\pi}{2}\right), \tag{74}$$

$$\Omega_2(m,n) = \frac{\partial\phi(m,n)}{\partial n} = \frac{2\pi}{3} + \frac{\pi}{6}\cos\left(\frac{\pi}{30}n\right). \tag{75}$$

Note that the carrier frequency along each direction is $\frac{2\pi}{3}$. Hence the IF components of the image are out of the range $[0, \frac{\pi}{2}]$. The demodulation results for the DHODA and the BMFT-DHODA are illustrated in Fig. 12. Specifically, Fig. 12 contains perspective plots of the IF estimation for the wideband sinusoidal example where IF components are out of the range $[0, \frac{\pi}{2}]$ via the DHODA and

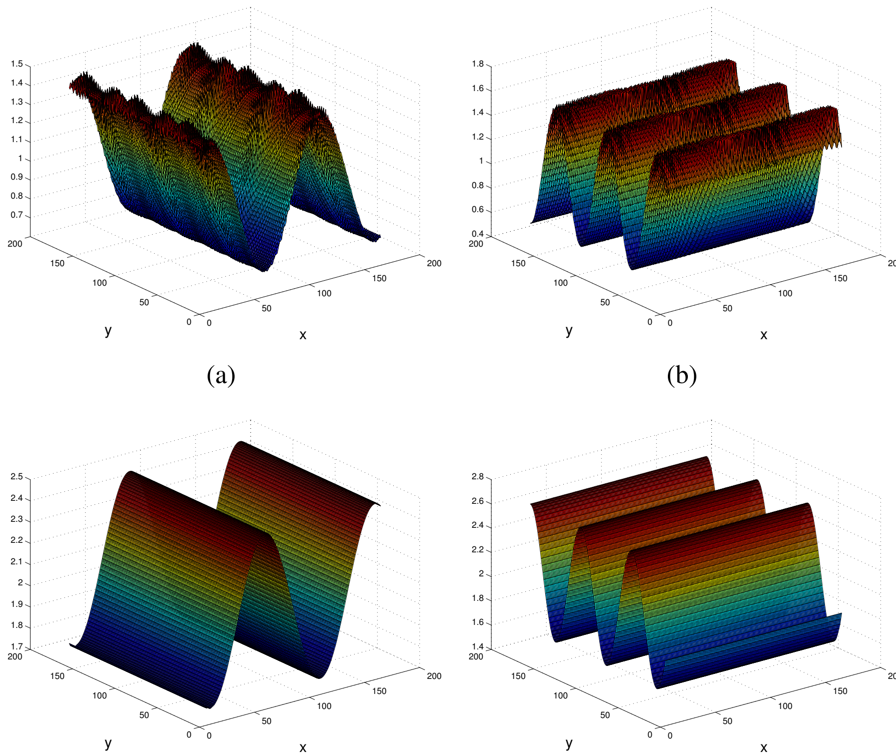

(a) (b) (c) (d)

Figure 12: Perspective plot of the IF estimation for the wideband sinusoidal example where IF components are out of the ESA estimation range via the DHODA and via the BMFT-DHODA

---

via the BMFT-DHODA with conversion factors $\vec{R} = \mathrm{diag}[8, 8]$. Fig. 12(a) is an estimation of the IF component along the horizontal direction via the DHODA. Fig. 12(b) is an estimation of the IF component along the vertical direction via the DHODA. Fig. 12(c) estimation of the IF component along the horizontal direction via the BMFT-DHODA. Fig. 12(d) is an estimation of the IF component along the vertical direction via the BMFT-DHODA. As we can observe, the demodulated IF components via the DHODA are seriously distorted in both amplitudes and phases, whereas the demodulated IF components via the BMFT-DHODA are smooth and valid. The RMSE for the DHODA is as large as 56.74% while the RMSE for the BMFT-DHODA is merely 0.9113%. Hence our claim that the BMFT helps overcome the range constraint of demodulation algorithms based on ESA is justified.

In the third experiment, we justify the efficacy of the proposed BMFT approach on real images. The real image of an oakring (photo by H.D. Grissino-Mayer) is shown by Fig. 13(a) where (a) is Real image of the oakring, (b) is the estimation of the IF component along the horizontal direction via the DHODA, (c) is the estimation of the IF component along the vertical direction via the DHODA, (d) is the estimation of the IF component along the horizontal direction via the BMFT-DHODA, (e) is the estimation of the IF component along the vertical direction via the BMFT-DHODA, (f) is the estimation of the IF needle plot via the DHODA, (g) is the estimation of the IF needle plot via the BMFT-DHODA, (h) is the estimation of the IA via the DHODA, and (i) is

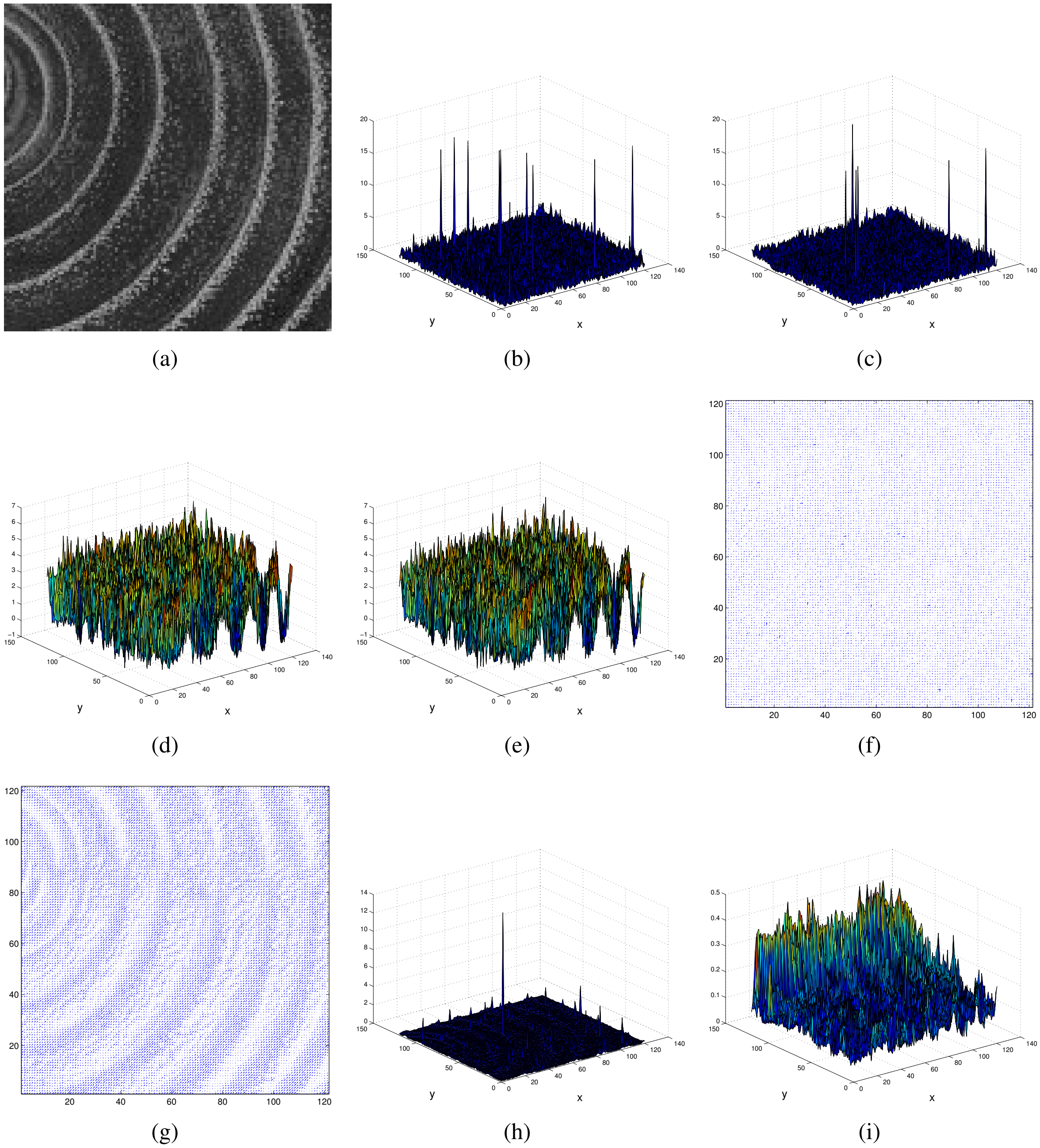

Figure 13: Demodulation of the oakring image (photo by H.D. Grissino-Mayer)

the estimation of the IA via the BMFT-DHODA. Note that the conversion factors of the BMFT-DHODA here are $\vec{R} = \mathrm{diag}[16, 16]$. The demodulation results associated with this real oakring image are compared in Fig. 13. The estimated IF components via the DHODA, as shown in Fig. 13(b) and Fig. 13(c), have singular points with significantly large values. The estimated IF components via the BMFT-DHODA, as shown in Fig. 13(d) and Fig. 13(e), are much smoother and do not have any singular point with significantly large value. As a result, the estimated IF needle plot of the DHODA (Fig. 13(f)) is seriously distorted by those singular points, whereas the estimated IF needle plot of the BMFT-DHODA (Fig. 13(g)) reveals the ring pattern corresponding

to the real oakring image. Note that the IA estimated via the DHODA (Fig. 13(h)) suffers from the same issue whereas the IA estimated via the BMFT-DHODA (Fig. 13(i)) does not. We see that ESA demodulation employed by the DHODA prohibits its direct application to wideband real images due to the narrowband and estimation range constraints, while the proposed BMFT framework allows for direct application of ESA demodulation to wideband real images.

4.2 Wideband Hypernasal Speech Demodulation

Formant analysis has found various applications in fields such as speech synthesis, bandwidth compression and speech transmission. Formants are natural resonances of the vocal tract and each formant is generally modeled as an AM-FM signal [2]. The goal of formant analysis here is to demodulate the IF and the IA of the corresponding formant. But first of all, we need to isolate each formant from the speech signal, which is conventionally achieved via bandpass filtering. However, by using bandpass filtering, the center frequency and bandwidth are manually assigned to each formant, which may incur serious distortion to the isolated resonance signal and result in inaccurate tracking of the IF and IA of the corresponding formant. In addition, wideband formants may overlap with each other in the spectrum, therefore they cannot be simply isolated via bandpass filtering.

In this section, we primarily focus on the first formants of the vowels, which are generally wideband due to the small center (or carrier) frequency, especially the nasal vowels. We propose the Empirical Mode Decomposition (EMD) [17] instead of bandpass filtering for the first formant extraction and apply the MFT approach to demodulate the IA and IF of the wideband first formant for further analysis.

4.2.1 Empirical Mode Decomposition

The EMD algorithm is an intuitive method that perform decomposition process adaptively with an posteriori defined basis derived from the data itself. It generally involve two major procedures, namely the sifting process and decomposition.

4.2.2 Sifting Process

A function is called an intrinsic mode function (IMF) if the following conditions are satisfied: 1) The number of extremas and the number of zero crossings equals or differs at most by one; 2) the average of the upper envelope defined by local maximas and the lower envelope defined by local minimas at any point is zero. The IMF reflects the oscillation mode inherent in the signal. It can be modeled as AM-FM and is not restricted to narrowband signal.

The sifting process is a systematic way to extract the IMF from the input data $x(t)$ and can be summarized via

- Initialize $d_0(t) = x(t)$
- Identify the local extremas of $d_n(t)$.
- Interpolate the local maximas and local minimas to form the the upper envelope $u_n(t)$ and lower envelope $v_n(t)$ respectively.
- Determine the local mean of the upper and lower envelopes $m_n(t) = \frac{u_n(t)+v_n(t)}{2}$.
- Extract the detail: $d_{n+1}(t) = d_n(t) - m_n(t)$.
- Repeat from step 2 to step 5 until $d_{n+1}(t)$ is an IMF (zero mean or stopping criterion met).

4.2.3 Decomposition

Assume that the signal $X(t)$ is composed of a few oscillatory modes that can be modeled by the IMF. Decomposition is a procedure that keep repeating the sifting process to decompose the signal as the sum of a few IMFs plus a residue described by

$$X(t) = \sum_{k=1}^{n} c_k + r_n, \tag{76}$$

where $c_k(t)$ denotes the corresponding IMF and $r_n(t)$ denote the final residue.

The decomposition procedure is summarized via

- Initialize $r_0(t) = X(t)$.
- Apply the sifting process on $r_n(t)$ to obtain the corresponding IMF $c_{n+1}(t)$ and the residue $r_{n+1}(t) = r_n(t) - c_{n+1}(t)$.
- Repeat the previous step until the residue $r_{n+1}(t)$ has no more extremas or meets the stopping criterion.

4.2.4 EMD Analysis

According to the structure of the EMD, the number of extrema associated with the extracted IMF is gradually decreased iterating from one residue to the next in the decomposition procedure. It corresponds to a filterbank structure with subband changing from high frequency range to low frequency range. However, it is different from any predetermined subband filtering, since the frequency range and resolution associated with each subband are adaptively time-varying. It offers more flexibility than the traditional multiband filtering approach in capturing features that are nonstationary.

Except the basic EMD algorithm reviewed in previous sections, there are a few variants such as the ensemble empirical mode decomposition (EEMD) [19]. The key idea of the EEMD relies on averaging the modes obtained by applying EMD to different realizations of Gaussian white noise added to the original signal. By introducing white Gaussian noise, the mode mixing problem can be solved via populating the whole time-frequency space to take advantage of the dyadic filter bank behavior of the EMD.

Currently, we only employ the basic EMD to obtain the first formant of the vowel for the purpose of illustration. In the future, we intend to apply other variants of the EMD algorithm such as the EEMD with adaptive noise to see if better results can be achieved.

4.2.5 First Formant Extraction via EMD

Formants are natural resonances of the vocal tract and have considerable amounts of amplitude and frequency modulation. Speech quality may deteriorate significantly when the modulations are removed. The center frequency and bandwidth of the formant associated with any given vowel varies from person to person. In addition, the first formant usually lies in the low-frequency range and has a relatively small center frequency to bandwidth ratio. Therefore it is generally considered as a wideband formant. In this effort, the EMD is preferred over bandpass filtering as the technique to extract the first formant due to the following reasons: 1) EMD does not require accurate estimation

for the center frequency and bandwidth of the first formant, which is hardly accessible via Linear Predictive Coding (LPC) or other methods. 2) EMD allows for some amount of spectrum overlap between the first formant and the second formant.

To extract the first formant, we perform the EMD on the speech signal $S(t)$ to obtain the IMFs and the residue through

$$S(t) = \sum_{k=1}^{n} c_k(t) + r_n(t). \tag{77}$$

By choosing an appropriate number m, we can ignore the first m IMFs that locate in the high-frequency range of the spectrum and sum up the rest of the IMFs plus the residue to obtain the first formant via

$$F_1(t) = \sum_{k=m+1}^{n} c_k(t) + r_n(t). \tag{78}$$

We can see that the first formant extraction via the EMD does not require any estimation for the center frequency and the bandwidth. It is simple to choose an appropriate number m by observing the oscillation mode of each IMF. In addition, since each IMF is modeled as AM-FM signal, some amount of spectrum overlapping between the first formant and the second formant is allowed.

4.2.6 Example of The First Formant Demodulation via the MFT approach

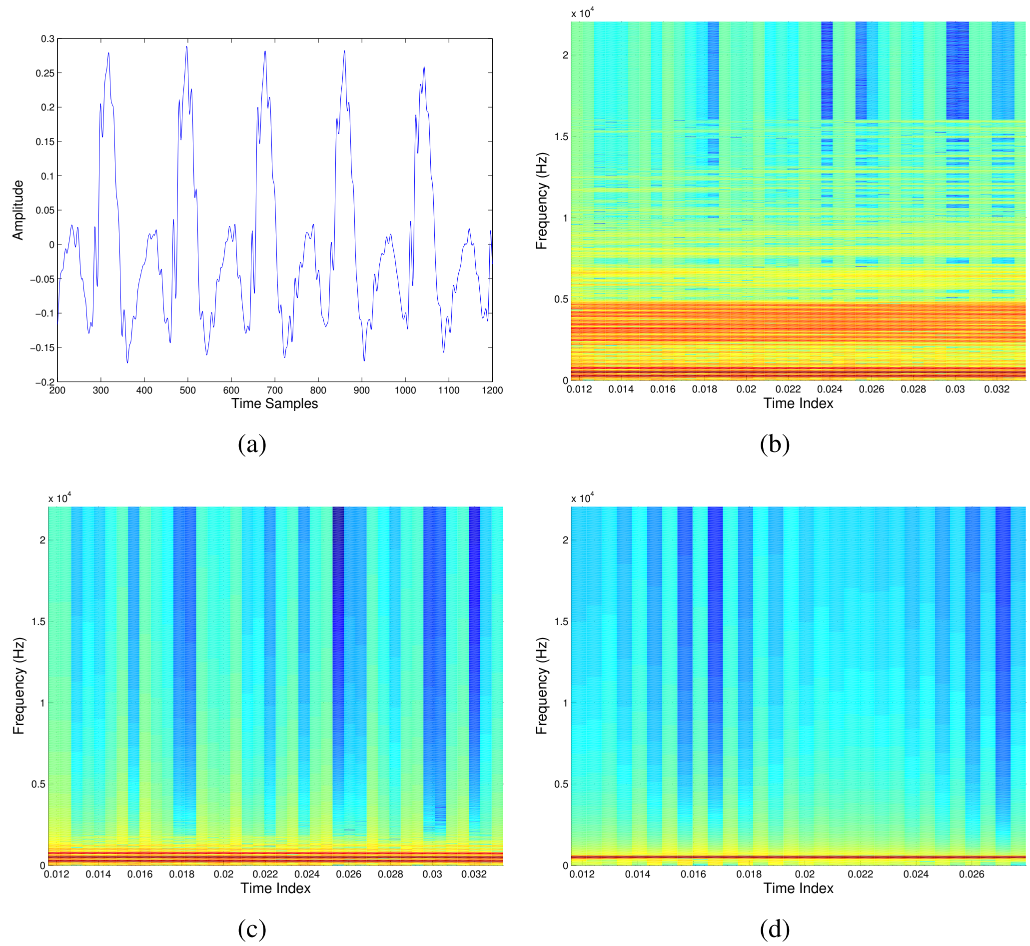

Figure 14: Example of the wideband first formant extraction via EMD

In this section, we present an example of the demodulation of the first wideband formant. The speech waveform and the corresponding short-time spectrum of an women's nasal vowel /iy/ (sample collected by Christopher) is shown by Fig. 14(a) and Fig. 14(b) respectively. The first formant of this vowel is obviously wideband, with a relatively small center frequency but a large bandwidth. The short-time spectrum of the first formant extracted via the EMD as we previously propose is shown by Fig. 14(c). For comparison, the short-time spectrum of the first formant extracted via bandpass filtering using LPC estimation of center frequency and bandwidth is shown by Fig. 14(d). Since the LPC estimation approach is only valid for narrowband signals, the estimated bandwidth of the first formant is very small, thus leading to inaccurate extraction of the first formant. On the other hand, the distortion of the first formant extracted via the EMD is very small compared to the original spectrum.

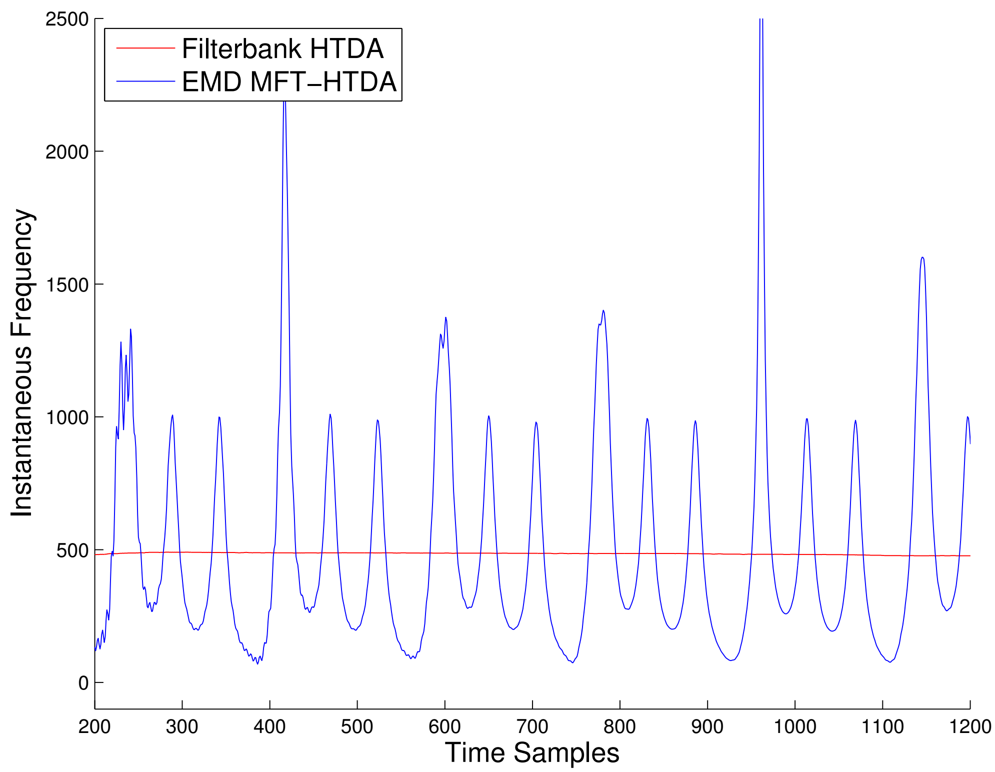

Figure 15: IF demodulation of the first formant

Since the first formant in this example is wideband, we apply the MFT and Hilbert transform combination as the demodulation scheme to obtain the IF. The IF demodulation of the first formant is illustrated in Fig. 15. The blue line corresponds to the IF demodulated via MFT and Hilbert transform using the first formant extracted via the EMD. For comparison, the red line corresponds to the IF demodulated via the Hilbert transform alone using the first formant extracted via bandpass filtering in conjunction with LPC estimation of the center frequency and bandwidth. As we can observe, the IF demodulated from the first formant extracted via bandpass filtering is almost a straight line, reflecting the fact that the bandpass filtering with LPC estimation only works under the narrowband scenario, whereas the IF demodulated using the MFT and Hilbert transform combination keeps allows for tracking the IF variation of the first formant in a much wider range.

4.3 Wideband CPM Demodulation for Satellite Communications

Wideband FM demodulation is a popular technique for satellite communications due to its ability to deal with trans-ionospheric distortion [3]. Contemporary methods for the demodulation of wideband FM signals either use negative feedback [2] or frequency estimation, or multirate frequency transformations and adaptive frequency tracking [4]. A particular form of digital FM, multilevel Gaussian Frequency Shift Keying (FSK) has been proposed as a solution for high bandwidth satellite communications.

On the wireless communication front, continuous phase modulation (CPM) belongs to a class of non linearly modulated signals with constant envelope, where the information is carried in the phase of the transmitted signal. High spectral efficiency and suitability to non linear class C amplifiers used in mobile radio applications make CPM a popular modulation choice. A specific form of CPM namely Gaussian minimum shift keying (GMSK) has been adopted in the Global System for Mobile communications (GSM) [21, 22]. The optimum receiver structure for CPM demodulation employs the maximum likelihood (ML) detector based on the Viterbi algorithm [18, 21, 22]. This receiver structure, however has significant computational complexity which grows exponentially with increase in the number of phase states.

In prior work [5, 8], it was shown that frequency discrimination for full response CPM demodulation has the same performance as that of binary phase shift keying (BPSK) detection in AWGN. In recent work [4] frequency tracking based wideband FM demodulation was extended to large wideband to narrowband conversion factors using multirate frequency transformations. Frequency estimation based approaches have the added advantage that they are immune to phase distortions introduced by the channel which would affect the Vitterbi approach. In this section, we apply the MFT enabled wideband FM demodulation approach to CPM demodulation. The first step is the adaptive linear predictive tracking of the instantaneous frequency of the CPM waveform using a gradient based adaptive step-size normalized least mean squares (LMS) algorithm [7] and multirate frequency transformations.

4.3.1 CPM Signal Model

For discussion purposes, we will adopt a rectangular pulse-shaping function $p(t)$ with a duration of L symbol periods and binary Pulse amplitude Modulation (PAM) symbols $a[k] \in \{-1, 1\}$. The

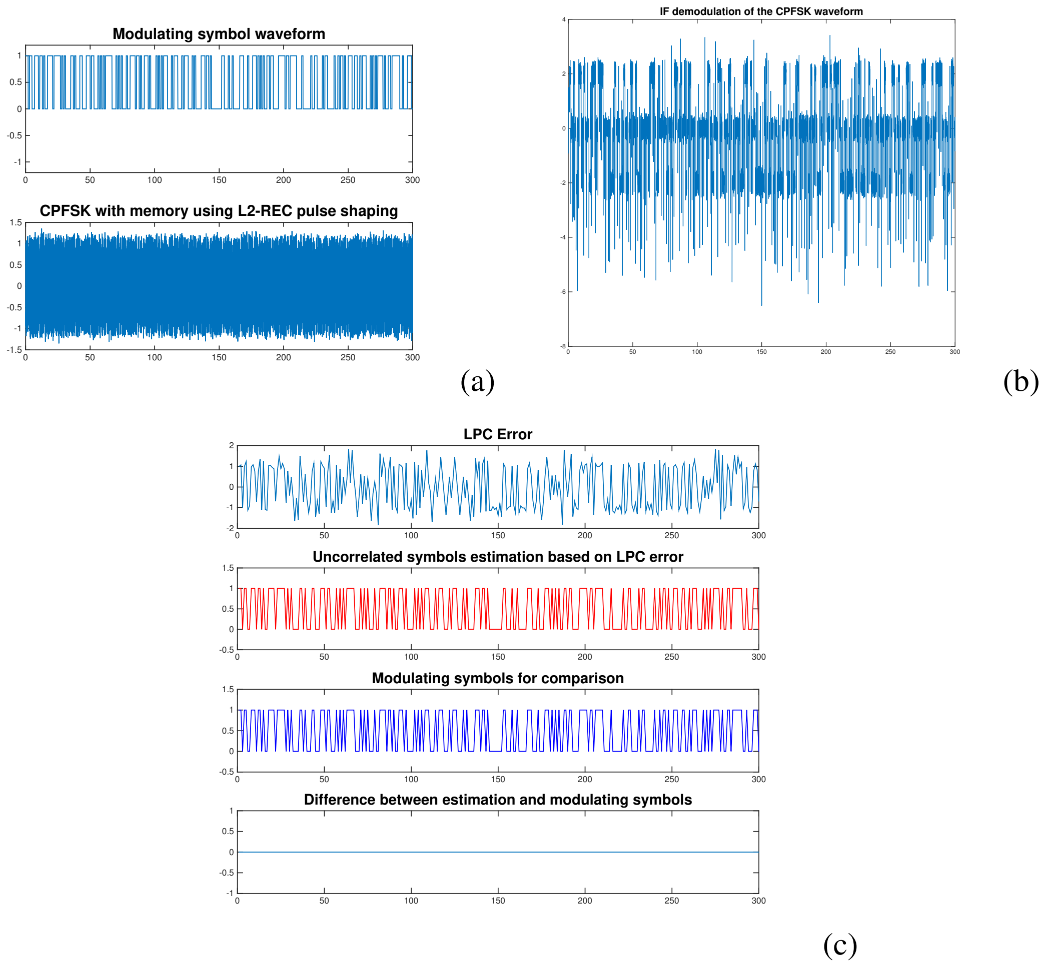

Figure 16: Two-stage linear prediction approach for CPFSK demodulation

---

IF signal in either case takes the form:

$$\omega_i(t) = \omega_c + 2\pi h \sum_{k=-\infty}^{\infty} a[k]p(t - kT_b), \tag{79}$$

where ω_c is the carrier frequency and h is the modulation index of CPM. The phase deviation from the carrier phase is given by:

$$\phi_{dev}(t; \mathrm{a}) = 2\pi h \sum_{k=-\infty}^{\infty} a[k]q(t - kT_b), \tag{80}$$

where $q(t) = \int_0^t p(\tau)d\tau$ corresponds to the phase pulse shaping function. The CPM signal is then obtained via frequency modulation:

$$r(t) = A\cos\left(\int_{-\infty}^{t} \omega_i(\tau)d\tau + \theta_0\right). \tag{81}$$

Using a pulse shaping function of duration larger than a symbol period introduces memory into the modulation scheme (LREC-CPM). In this report, we will focus our attention on the memoryless case with $L = 1$, i.e., (1REC-CPM). Specifically CPM with a rectangular pulse of one symbol duration (1-REC-CPM) is equivalent to continuous phase frequency shift keying (CPFSK). Another form of CPM, minimum shift keying (MSK), is equivalent to 1-REC-CPM with $h = 0.5$, while GMSK can be put into the CPM framework with a Gaussian pulse function. The results of which are shown in Fig. 16 where (a) is the modulating bits and corresponding CP-FSK waveform for 2-REC CPM at a SNR of 13 dB, (b) is the IF estimate from the first stage of adaptive linear prediction, and (c) is the removal of memory induced by partial response signaling using a second-stage of linear prediction.

4.3.2 Wideband CPM Demodulation

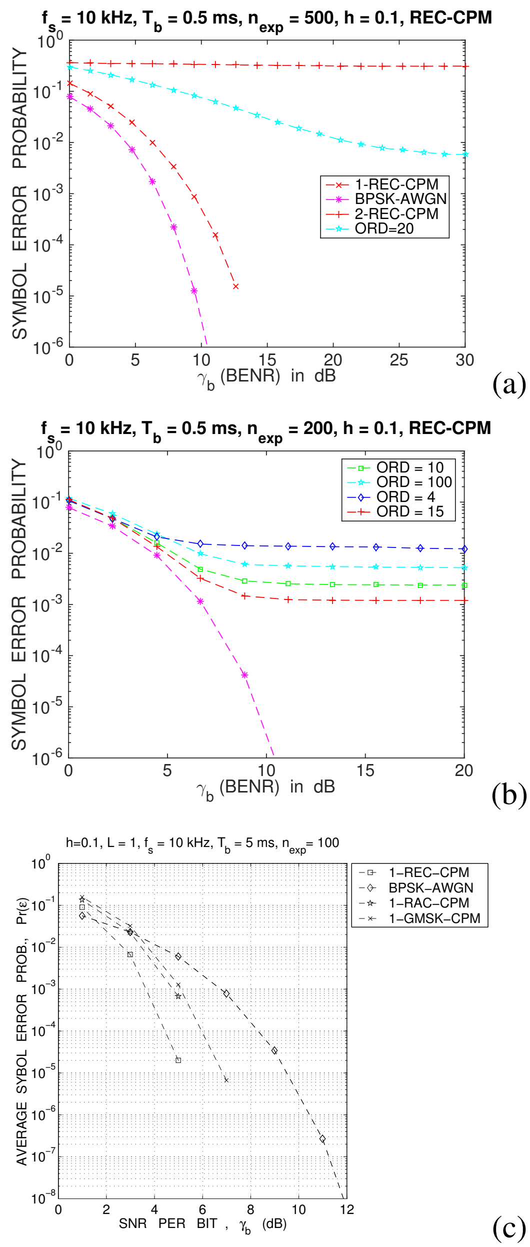

Figure 17: Performance of the dual stage linear prediction approach

---

In prior work [4], we have applied various forms of adaptive filtering to the demodulation of CPM signals without memory. It was shown that oversampling results in an improved performance analogous to that of binary detection in AWGN. When partial response signaling is employed, this induces ISI in the estimated IF and a loss of performance. Figure 17 depicts the application of the wideband demodulation approach to CPM signals with memory, i.e., $L = 2$ CPM. As can be observed, partial response signaling induces ISI and a deterioration in performance after averaging over 500 experiments. Specifically adjusting the predictor order allows for removal of more of the

memory induced ISI. Within Fig. 17, (a) is for $L = 2$-REC CPM using a $p = 20$-th order predictor Partial response signaling induced ISI results in a error floor that can be mitigated to a certain extent by the second stage of linear prediction, (b) is the effect of predictor order in the second stage on the performance of the algorithm, and (c) is the effect of pulse shape with no memory. Specifically future work will focus on the following: (a) the effect of channel memory on the performance of the proposed approach, (b) effect of predictor order on performance, and (c) effect of pulse shape on the performance of the algorithm. Equalization efforts such as decision feedback equalization [18] applied directly to the estimated IF can be used to further aid in the reduction of the ISI.

5 Conclusion

In this report, we have presented an extension of the recently proposed [4] MFT based wideband FM demodulation approach to large wideband to narrowband demodulation factors, thereby enabling more practical implementations of the filters internal to the heterodyne and interpolation modules. It was shown that this approach significantly reduces the demodulation errors in comparison to direct application of the narrowband approaches.

We further extended the MFT approach to two dimensions and combined it with demodulation approaches based on higher-order two-dimensional Teager-Kaiser energy operators. When applied to both synthetic and natural wideband images to demonstrate that significant reduction of demodulation errors over just narrowband demodulation algorithms. When applied to wideband formants encountered in hypernasal situations, the wideband demodulation approach provides more accurate estimates of the instantaneous frequency of the first formant over linear prediction approaches that filter out a lot of the valuable sidelobe information.

When then applied the proposed approach to the problem of wideband CPM demodulation, the approach with oversampling was shown to provide a performance similar to that of binary detection in AWGN in the memoryless situation. For symbols with memory, linear prediction of the IF estimates removes some of the induced memory, but further equalization in the form of minimum mean squared error or decision feedback equalization [18] of the estimated instantaneous frequency is needed to completely remove the memory.

References

[1] A. Potamianos and P. Maragos, "A comparison of the energy operator and the Hilbert transform approach to signal and speech demodulation," Signal Processing, Vol. 37, No. 1, pp. 95 - 120, 1994.

[2] P. Maragos, J. F. Kaiser, and T. F. Quatieri, "Energy separation in signal modulations with application to speech analysis," *IEEE Transactions on Signal Processing*, Vol. 41, No. 10, pp. 3024 - 3051, Oct 1993.

[3] E. Bedrosian, "Trans-ionospheric propagation of FM signals," RM-5369- NASA, RAND Memorandum, August 1967.

[4] Balu Santhanam, "Generalized Energy Demodulation for Large Frequency Deviations and Wideband Signals," IEEE Signal Processing Letters, Vol. 11, No. 3, pp. 341-344, 2004.

[5] S. S. Haykin, "Adaptive Filter Theory," *Fourth Edition*. Upper Saddle River, NJ: Prentice Hall Press, 2005.

[6] L. J. Griffiths, "Rapid measurement of digital instantaneous frequency," *IEEE Trans. Acoust., Speech, Signal Process.*, Vol. 23, No. 2, pp. 207 - 222, 1975.

[7] D. Mandic, "A generalized normalized gradient descent algorithm," IEEE Signal Processing Letters, Vol. 11, No. 2, pp. 115-118, 2004.

[8] A. V. Oppenhein and R. W. Schafer, "Discrete-time signal processing," Second Edition, Prentice Hall, New York, 1999.

[9] F. F. Kuo and J. F. Kaiser, "System analysis by digital computer," John Wiley Publication, 1966.

[10] B. Santhanam, "Orthogonal modes of frequency modulation and the Sturm-Liouville frequency modulation model," *IEEE Trans. Signal Process.*, Vol. 60, No. 7, pp. 3486 - 3495, July 2012.

[11] F. Salzenstein, A.-O. Boudraa, and T. Chonavel, "A new class of multidimensional Teager-Kaiser and higher order operators based on directional derivatives," *Multidimensional Systems and Signal Processing*, pp. 1-30, 2013.

[12] M. S. Pattichis, G. Panayi, A. C. Bovik, and S.-P. Hsu, "Fingerprint classification using an AM–FM model," IEEE Transactions on Image Processing, Vol. 10, No. 6, pp. 951-954, Jun 2001.

[13] A. Bovik, N. Gopal, T. Emmoth, and A. Restrepo, "Localized measurement of emergent image frequencies by Gabor wavelets," *IEEE Transactions on Information Theory*, Vol. 38, No. 2, pp. 691 - 712, March 1992.

[14] P. Maragos and A. C. Bovik, "Image demodulation using multidimensional energy separation," *J. Opt. Soc. Am. A*, Vol. 12, No. 9, pp. 1867 - 1876, Sep 1995.

[15] M. Pattichis and A. Bovik, “Analyzing image structure by multidimensional frequency modulation,” *IEEE Transactions on Pattern Analysis and Machine Intelligence*, Vol. 29, No. 5, pp. 753 - 766, May 2007.

[16] F. Salzenstein, A.-O. Boudraa, and J.-C. Cexus, “Generalized higher-order nonlinear energy operators,” J. Opt. Soc. Am. A, Vol. 24, No. 12, pp. 3717-3727, Dec 2007.

[17] N. E. Huang, Z. Shen, S. R. Long, M. C. Wu, H. H. Shih, Q. Zheng, N.-C. Yen, C. C. Tung, and H. H. Liu, “The empirical mode decomposition and the Hilbert spectrum for nonlinear and non-stationary time series analysis,” *Proceedings of the Royal Society of London*, Series A: Mathematical, Physical and Engineering Sciences, Vol. 454, No. 1971, pp. 903 - 995, 1998.

[18] J. G. Proakis and Masoud Salehi, “Digital Communications,” Fifth edition, McGraw-Hill Publishing Company, New York, 1995.

[19] Z. Wu and N. E. Huang, “Ensemble empirical mode decomposition: a noise- assisted data analysis method,” *Advances in adaptive data analysis*, Vol. 1, No. 01, pp. 1 - 41, 2009.

[20] P. Maragos and A. Potamianos, “Higher order differential energy operators,” IEEE Signal Processing Letters, Vol. 2, No. 8, pp. 152-154, Aug 1995.

[21] J. B. Anderson, T. Aulin and C-E. W. Sundberg, “Digital Phase Modulation,” Plenum, New York, 1986.

[22] C-E. W. Sundberg, “Continuous Phase Modulations Part I and II,” IEEE Communications Magazine, Vol. 24, pp. 25-38, April 1986.

LIST OF SYMBOLS, ABBREVIATIONS AND ACRONYMS

AF-RLS	Root Least Squares
AM-FM	Amplitude modulation frequency modulation
AS	Analytic signal
AS-LMS	Analytic Signal Least Mean Square
AWGN	Additive White Gaussian Noise
BEMD	Bi-dimensional Empirical Mode Decomposition
BMFT	Bi-dimensional multirate frequency transformation
BPF	Band Pass Filter
BPSK	Binary Phase Shift Keying
CPFSK	Continuous-Phase Frequency-Shift Keying
CPM	Continuous phase modulation
CR/FD	Carrier to frequency deviation ratio
CR/IB	Carrier to information bandwidth ratio
CRLB	Cramer-Rao lower bound
dB	Decibel
DCA	Dominant Component Analysis
DHODA	Discrete higher order demodulation algorithm
EEMD	ensemble empirical mode decomposition
EMD	Empirical Mode Decomposition
ESA	Energy separation algorithm
FIR	Finite Impulse Response
FSK	Frequency Shift Keying
GMSK	Gaussian minimum shift keying
GNGD	Generalized normalized gradient descent
HT	Hilbert transform
HTDA	partial Hilbert transform alone
IA	Instantaneous amplitude
IF	Instantaneous frequency
IFGT	instantaneous frequency gradient tensor
IMF	intrinsic mode function
LMS	Least Mean Squares
LPC	Linear predictive coding
MFT	Multirate frequency transformation
MSK	Minimum shift keying
NLMS	Normalized Least Mean Squares
NRMSE	Normalized Root Mean square error
PAM	Pulse Amplitude Modulation
RMSE	Root Mean Square Error
SNR	Signal to Noise Ratio

DISTRIBUTION LIST

DTIC/OCP 8725 John J. Kingman Rd, Suite 0944 Ft Belvoir, VA 22060-6218	1 cy
AFRL/RVIL Kirtland AFB, NM 87117-5776	2 cys
Official Record Copy AFRL/RVSW/David Murrell	1 cy

(This page intentionally left blank)